

# Therapeutic Effect of Bone Marrow Derived Mesenchymal Stem Cells Versus their Exosomes on Isoproterenol Induced Ventricular Myocardium Changes in Adult Rats: A Histological, Immunohistochemical and Biochemical Study

Amany A. Solaiman and Rehab A. Abd El-Moneim

Department of Histology and Cell Biology, Faculty of Medicine, Alexandria University, Egypt

## ABSTRACT

**Introduction:** Myocardial infarction represents a life-threatening condition. The mechanisms involve the accumulation of reactive oxygen species and hypoxia. Immediate therapeutic intervention of bone marrow derived mesenchymal stem cells (BM-MSCs) and their exosomes have been investigated for their possible therapeutic effects to avoid cardiac remodeling and fibrosis.

**Aim of the Work:** To investigate the therapeutic potential of BM-MSCs versus their exosomes to influence the isoproterenol (ISO) induced myocardial changes in a rat model.

**Materials and Methods:** 32 adult male albino rats were divided into five groups: Control group, ISO group (received ISO in a dose of 85mg/Kg body weight subcutaneously, twice at 24 hours interval, and sacrificed four weeks after the last dose), exosomes and stem cells treated groups (injected via the tail vein by 100µg of exosomes or  $1.2 \times 10^6$  of BM-MSCs respectively, 24 hours after the last dose of ISO and sacrificed after four weeks) and recovery group (received ISO, left for four weeks after the last dose of ISO, then sacrificed). Samples from the left ventricle were processed for histological assessment using light and electron microscopes. Immunohistochemical assessment of anti-caspase-3 was included. The right ventricles were homogenized for assessment of malondialdehyde, total antioxidant capacity, tumor necrosis factor- alpha and transforming growth factor beta1. Troponin I and creatine kinase were also assessed in the serum.

**Results:** Histologically, the ISO group revealed degenerative changes in the form of myocytolysis, cellular infiltration and nuclear changes. Serum levels of Troponin I, and Creatine kinase were significantly increased. Significant increase in the anti-caspase-3 reaction was demonstrated morphometrically. Both exosome and stem cell groups revealed improvement in different assessed parameters that was more evident in the exosome treated group.

**Conclusion:** Exosomes proved to demonstrate more potent therapeutic effect as compared to BM-MSCs on isoproterenol induced ventricular myocardium change, thus regarded as a promising therapeutic strategy in myocardial infarction.

**Received:** 01 December 2021, **Accepted:** 10 January 2022

**Key Words:** Exosomes, myocardial infarction, remodeling, stem cells.

**Corresponding Author:** Rehab Ahmed Abd El-Moneim, PhD, Department of Histology and Cell Biology, Faculty of Medicine, Alexandria University, Egypt, **Tel.:** +20 10 0109 2769, **E-mail:** rehabahmed2013.ra@gmail.com

**ISSN:** 1110-0559, Vol. 46, No. 2

## INTRODUCTION

Ischemic heart disease and associated myocardial infarction (MI) are regarded as one of primary causes of death worldwide as documented by the World Health Organization (WHO)<sup>[1]</sup>. The extent of cellular injury, and/or death after ischemia might cause irreversible cardiomyocyte damage. The mechanisms of such damage involve lack of oxygen and nutrients, calcium overload, and accumulation of reactive oxygen species (ROS)<sup>[2]</sup>. Moreover, an inflammatory response is stimulated along with MI, where production of inflammatory cytokines and infiltration of immune cells into the ischemic area occur, thereby result in exaggerated cardiac remodeling, fibrosis, and ultimately end by heart failure<sup>[3]</sup>.

Impeding coronary blood flow is a prominent reason for myocardial injury and infarction, this is referred to as Type 1 MI (T1MI). On the other hand, Type 2 MI (T2MI) occurs

in the absence of coronary artery disease and estimates up to 58% of MI patients<sup>[4,5]</sup>. Several factors have been suggested to cause this nonischemic myocardial injury including elevated circulating levels of inflammatory cytokines, combined with marked electrolyte abnormalities<sup>[4]</sup>.

Rodents are consistently used for experimental induction of myocardial injury and infarction. One of the most widely used techniques is the surgical ligation of the left anterior descending artery, an insidious procedure associated with high mortality rates in the experimental animals. The induction of cardiomyocyte necrosis and fibrosis by using the isoproterenol (ISO) is remarkably useful for averting the increased mortality rates in animals and permitting a significant reduction of group sizes with animal welfare benefits<sup>[6]</sup>.

Isoproterenol, a non-specific  $\beta$ -agonist, causes serious myocardial ischemia, necrosis, and hypoxia. The

histological, physiological, as well as metabolic changes in the cardiomyocytes of experimental animals after ISO administration were reported to simulate those occurring in humans after myocardial ischemia<sup>[7,8]</sup>. That's why ISO was chosen in the current study rather than the commonly used surgical ligation for induction of a model of myocardial injury.

Strategies to improve tissue repair and prevent fibrosis are still arousing and intend to control both the inflammatory response and oxidative stress to preserve myocardial structure and function, taking into consideration the negligible regenerative capacity of the myocardium. Beyond these strategies, stem cell regenerative therapies were achieved. However, they are still facing challenges for clinical applications<sup>[9]</sup>. Accumulating studies have shown that bone marrow-derived mesenchymal stem cells (BM-MSCs), improved cardiac function after MI. However, most of the conducted research work, recorded unsatisfactory results, due to low engraftment rate and viability of the transplanted cells in the ischemic area, with subsequent restricted effect concerning remodeling and sustained contractile ability<sup>[10,11]</sup>.

Despite these challenges, one strategy that has received significant awareness is the exosomes (EXO) that provides various opportunities for treating heart diseases<sup>[12]</sup>.

Although several stem cells are considered as potential sources for secretion of EXO, yet BM-MSCs are regarded as the stem cells of choice. This is due to the more potent paracrine effect of MSCs, feasibility of isolation and culture, higher rate of proliferation and longevity of survival, as compared to other stem cells<sup>[13]</sup>. As such, BM-MSCs were the stem cells of choice in the current study. It has been demonstrated by a previous research work that the therapeutic potential of MSCs derived exosomes, involves inhibition of cardiomyocyte apoptosis, enhancement of survival and angiogenesis in rats post MI. Such cardioprotective effect of EXO is due to their contents of mainly different types of mi-RNAs, which can be modulated by controlling some parameters in the microenvironment of the BM-MSCs in culture<sup>[14]</sup>.

In the literature, EXO are a subtype of extracellular vehicles (EVs) transferring information between donor and target cells and hence regulate the function of recipient cells. The development of exosome-based therapy holds great promise for regenerating and repairing cardiomyocytes after damage. In this context, EXO became a field of much research interest, that aimed to investigate effective isolation techniques to adopt cell free regimens, depending on a bioactive paracrine mechanism<sup>[15]</sup>. The EXO are small nano-sized membrane bound structures (30-200 nm) formed by invagination of endosomes forming multivesicular bodies (MVBs). MVBs can move to the lysosome for degradation of vesicles and/or fuse with the cell membrane, eventually liberating their vesicles into the extracellular space as EXO. The released EXO will either be taken up by target cells dwelling in the microenvironment

around or transported distally via biological fluids. The EXO possess several advantages: they are more stable than the cells, biocompatible, circulate all through the body and cross the blood-brain barrier. Besides, they are resistant to freezing and thawing. In addition, EXO represent a safer therapeutic strategy as compared to stem cells, where they do not carry the risk of tumor formation or immune system reaction<sup>[16]</sup>.

Based on these considerations, this work innovatively aimed to study histologically and biochemically the therapeutic potential of BM-MSCs in comparison to their derived exosomes to influence the changes that might accompany myocardial injury in a rat model of T2MI using the isoproterenol.

## MATERIALS AND METHODS

### *Isolation and culture of BM-MSCs*<sup>[17]</sup>

All procedures used for isolation and characterization of BM-MSCs were accomplished at the Center of Excellence for Research in Regenerative Medicine and its Application (CERRMA), Faculty of Medicine, Alexandria University.

Under complete sterile condition, five Sprague-Dawley male rats (aging 3 weeks old, weighing 27–30 grams), were sacrificed in a vertical laminar airflow hood. The bone marrow suspension from the femurs was attained by flushing the bone marrow cavity utilizing a syringe (5 ml) and complete culture media (CCM) (low glucose Dulbecco's Modified Eagle Medium (LG-DMEM) (1.0 g/L glucose, Sigma-Aldrich, St. Louis, MO, USA). Filtration of the suspension using a 70 mm filter mesh was done and then centrifuged at 1200 rpm for 5 minutes. The cell pellets were resuspended in CCM enhanced with 10% Fetal bovine serum (FBS, Sigma-Aldrich), 1% L-glutamine (Lonza) and 1% Penicillin/ streptomycin (Lonza) in 25 cm<sup>2</sup> tissue culture flask and incubated in the CO<sub>2</sub> incubator at 37°C in a humidified atmosphere with 95% O<sub>2</sub> and 5% CO<sub>2</sub>. These cultured cells were considered as Passage 0 (P0). 48 hours later, any non-adherent cells were washed by phosphate buffered saline (PBS, Lonza, Bornem, Belgium). The CCM was changed every 48-72 hours and the non-adherent cells were discarded. While the adherent cells on reaching a confluence level of 70-80%, they were washed (PBS), detached with 0.25% trypsin/ ethylene diamine tetra-acetic acid (EDTA) (Thermo Fisher Scientific, Waltham, MA) solution and split in a ratio of 1:3. When the cultured cells reached passage three (P3) they were used in the current study. Examination of the cultured cells was achieved using a phase-contrast inverted microscope supplied with a digital camera (Olympus CKX41SF, Tokyo, Japan).

### *Characterization of BM-MSCs*

#### **Immunophenotyping using flow cytometer**<sup>[18]</sup>

Immunophenotyping was performed on P3 cultured cells by applying fluorescent-labeled monoclonal antibodies for CD90, CD73, CD105, CD44, CD11b and CD45 surface

markers. Adherent cells were trypsinized using 0.25% trypsin-EDTA solution, washed, and incubated in the dark at room temperature for 30 minutes, with the designated antibodies. Monoclonal Allophycocyanin-conjugated antibody specific for CD90 (Anti-Thy1.1) (Abcam, Cambridge, UK), monoclonal FITC-conjugated antibody specific for CD73 (Abcam, Cambridge, UK) were used. In addition, monoclonal PE-conjugated antibody specific to CD105 (Abcam, Cambridge, UK), CD44 phycoerythrin PE-conjugated antibody (Abcam, Cambridge, UK), CD11B PE-conjugated (Abcam, Cambridge, UK) and monoclonal phycoerythrin (PE)-conjugated antibody for CD45 (Abcam, ab23396, UK), were also performed. Cells were washed three times with PBS and resuspended in 500 ml fluorescence activated cell sorting (FACS) buffer. For assessment of immunofluorescence on the viable cells, a Caliber flow cytometer equipped with Cell Quest software (Becton Dickinson, New Jersey, USA), was used.

#### Colony-forming unit fibroblast assay (CFU-F)<sup>[19]</sup>

Plating of 100 cells on a six well plate in CCM was done, followed by 14 days of incubation to perform the CFU-F assay, Media was changed every 48–72 hours for 14 days. Next, the cells were washed (PBS), and stained with Crystal Violet (Sigma- Aldrich, USA) at 3% (w/v) in 100% methanol. The colonies displaying five or more cells in each well were counted using the inverted microscope. The “CFU potential” was calculated as equal to the number of colonies formed/number of cells plated x 100. The CFU potential over 40% was the most favorable for MSCs culture.

#### MSCs labeling and tracing<sup>[20]</sup>

For tracing the MSCs cells,  $1.2 \times 10^6$  MSCs/ml were labeled with a fluorescent probe (chloroma-ethyl-benzamide-octadecyl indocarbocyanines (CM-DiI) (molecular probes, Thermo Fisher USA). Labeled cells were injected into two rats, 24 hours after last dose of ISO via the tail vein under anesthesia. 72 hours after injection, rats were sacrificed and the heart from each rat was dissected removed and processed to obtain (5-6  $\mu$ m) thin sections from paraffin blocks for examination and image capturing using fluorescent microscope (Olympus BX41), and digital camera (Olympus DP20, Tokyo, Japan).

#### Isolation and characterization of MSCs-Extra cellular vesicles (EVs)

##### Isolation of MSCs-EVs<sup>[21]</sup>

When the P3 cultured cells displayed 80% confluence, they were cultured in serum-free media for 48 hours, followed by the collection of the culture media to isolate the EVs. Centrifugation of the collected media was applied at 300 rpm at room temperature for five minutes to separate any cell debris. The supernatant was further centrifuged at high-speed 3000 rpm at room temperature for 40 minutes. To make certain of removal of the large sized vesicles, filtration of the supernatant via a 0.2 $\mu$ m filter was done. For isolating MSCs-EVs, ultracentrifugation (Beckman

Coulter Optima L-100 K ultracentrifuge, Fullerton, CA, USA) at 130,000 rpm at 4 °C for 90 minutes was performed at the Research Institute Center, Alexandria University. Pellet was resuspended in PBS and divided into aliquots for characterization and injection into the respective group in the current study.

##### Characterization of MSCs-EVs

- EVs quantification using a protein assay<sup>[22]</sup>: EVs were quantified by assessment of the isolated samples' total protein content by Lowry method at the Biochemistry Department, Faculty of Medicine, Alexandria, University.
- Zita sizing (Malvern, UK)<sup>[23]</sup>: At the central lab, Faculty of Pharmacy, Alexandria University, the sample of the EVs was diluted using PBS then sonicated to avoid particles aggregates and finally placed in the zeta sizer sampling tube to measure the particles' size using Malvern Analytical Software UK.
- Transmission electron microscope (TEM)<sup>[24]</sup>: 20 $\mu$ l solution of EVs were diluted in 100  $\mu$ l PBS, the suspension was overloaded on copper grids, stained with uranyl acetate followed by examination using the TEM (JEM-1400 plus, Tokyo, Japan) at the Electron Microscopy Unite, Faculty of Science, Alexandria University.
- Western blot characterization of exosomes<sup>[25]</sup>: It aimed to determine the CD63 and CD81 membrane-associated proteins that indicate the endosomal origin of the isolated exosomes. This was performed at the Medical Biochemistry and molecular biology Department, Faculty of medicine, Cairo University. 20  $\mu$ g protein concentration of each sample of the EVs and MSCs pellets were loaded in equal volumes (PH 6.8). Then boiled (95°C for 5 minutes), loaded on polyacrylamide gel electrophoresis and the blot was run for 7 minutes at 25 V using BioRad Trans-Blot Turbo (California, USA). The membrane was blocked with Tween® 20 buffer and 3% bovine serum albumin at room temperature for one hour. In the following step, membranes were incubated overnight at 4 °C with the primary antibody (1:1000 dilution) for CD63 and CD81 (Santa Cruz Biotechnology, California, USA) and  $\beta$ -actin antibody (Abcam, Cambridge, UK), a housekeeping protein. Membranes were washed and incubated for one hour with horseradish peroxidase (HRP)-conjugated secondary antibody Goat anti-rabbit IgG (Biologicals, Ireland, UK) solution against the blotted target protein. The chemiluminescent substrate (Clarity™ Western ECL substrate Bio-Rad) was applied to the blot. Using a CCD camera-based imager, the signals were recorded. Image analysis software was used to read the band intensity of each of the target proteins against the control sample beta actin by protein normalization on the ChemiDoc MP imager.

### Experimental design

This experiment was conducted on 32 Sprague Dawley adult male albino rats (10-12 weeks old and 150-180 grams weight). Rats were acclimatized for two weeks before the experiment and were housed under a 12-hour light-dark cycle with food and water supplied ad libitum. Experiment was performed in accordance with the approved guidelines determined by the Research Ethics Committee of Alexandria Faculty of Medicine, Egypt. IBR number 00012098.

Isoproterenol (ISO) was purchased from Sigma-Aldrich (Saint Louis, USA) in a crystalline form with product number 16379.

Rats were randomly allocated into five main groups as follows:

**Group I:** Control (C) group: It included six rats, each rat received 1 ml/Kg body weight of physiological cold saline (vehicle of ISO), subcutaneously (SC), twice at an interval of 24 hours, and were sacrificed four weeks after last dose of saline.

**Group II:** Isoproterenol group (ISO): It included six rats. ISO at a dose of 85mg/Kg body weight was dissolved in cold saline and injected SC, twice at an interval of 24 hours, and were sacrificed 24 hours after the last dose of ISO<sup>[26]</sup>.

**Group III:** Exosomes treated group (EXO): It included six rats given ISO at a dose similar to group II. 24 hours after the second injection of ISO, each rat received a single IV injection (via the tail vein) of 100 µg exosome/rat in 100 µl CCM and were sacrificed after four weeks<sup>[27]</sup>.

**Group IV:** Stem cells treated group (ST): It included eight rats that were given ISO at a dose similar to group II. 24 hours after the second injection of ISO, six rats received  $1.2 \times 10^6$  MSCs in 1 ml CCM via the tail vein and were sacrificed after four weeks. Two rats were injected by the labeled stem cells and were sacrificed 72 h after injection for detection of homing of MSCs<sup>[28]</sup>.

Rats of EXO group III and ST group IV were anesthetized by intramuscular injection of 70mg/Kg ketamine (NEON lab, Mumbai, India) combined with 7mg/Kg xylazine (ADWIA Co. 10th of Ramadan city, Egypt) before the exosome and stem cell injections<sup>[29]</sup>.

**Group V:** Recovery group (R): It included six rats that were given ISO at a dose similar to group II. Rats were observed for spontaneous recovery for four weeks after the last dose of ISO, and then sacrificed.

### Tissue sampling

Animals in different experimental groups successfully survived the designated duration for each group, without any recorded deaths. All animals used in the current study were sacrificed at the designated time; each heart was dissected from all animals. Each heart was cut into

two nearly equal halves longitudinally. The right halves were homogenized in 1-2 ml of 5mM cold potassium phosphate buffer (pH 7.4), centrifuged at 4000 rpm for 15 minutes at 4°C and the supernatant was removed and stored at -80°C. Cardiac homogenates were used for assessment of malondialdehyde (MDA), total antioxidant capacity (TAC), tumor necrosis factor- alpha (TNF-α) and transforming growth factor beta 1 (TGF-β1). All were done at the Biochemistry Department, Faculty of Science, Borg El-Arab, Alexandria University.

### Biochemical study

On the day of tissue collection, 3 ml blood were collected from the retro-orbital plexus, centrifuged 10,000 rpm for 10 minutes at 4°C to get the serum, and eventually stored at -20 °C for later use to assess cardiac enzymes: cardiac Troponin I (cTnI), and creatine kinase- myocardial band (CK-MB). This was performed at the Physiology Department, Faculty of Medicine, Alexandria University

#### Cardiac Troponin I (cTnI)<sup>[30]</sup>

Assessment of cTnI was done using enzyme-linked immunosorbent assay (ELISA Kit, Bioneovan Co., Beijing, China) and expressed in picogram per milliliter (pg/ml).

#### Creatine kinase-MB (CK-MB)<sup>[31]</sup>

Assessment of CK-MB activity was performed using the diagnostic kit (Sigma-Aldrich, St. Louis, Missouri, USA). The increase in absorbance at 340 nm was measured to calculate CK-MB level (unite per liter (U/l)).

#### Malondialdehyde (MDA)<sup>[32]</sup>

This concerned the reaction of lipid peroxidation, malondialdehyde (MDA), with thiobarbituric acid (TBA), Bio diagnostics, kit Cairo, Egypt. Thiobarbituric acid reactive substances (TBARS) was generated, and the resulted red-pink color was measured at 532 nm. The concentration was expressed as nanomoles per milligram tissue protein (nmol/mg protein).

#### Total antioxidant capacity (TAC)<sup>[33]</sup>

Determination of TAC (Bio diagnostics, kit Cairo, Egypt) was achieved by the reaction of antioxidants in the sample with a known amount of hydrogen peroxide (H<sub>2</sub>O<sub>2</sub>). The leftover H<sub>2</sub>O<sub>2</sub> was measured calorimetrically that entails the conversion of 3, 5-dichloro-2-hydroxy benzene sulphonate to a colored product. The color change was measured at a wavelength of 505 nm. The concentration of TAC was expressed as nanomoles per milligram tissue protein (nmol/mg protein).

#### Tumor Necrosis Factor-alpha (TNF- α)<sup>[34]</sup>

In myocardial homogenate, analysis of TNF-α was performed according to the manufacturer's protocol (ELISA Kit, Abcam, Cambridge, UK). In brief, to each well the sample was added, and incubated (37°C for 90 minutes). Biotinylated anti-rat TNF-α antibody was added and incubated (37°C for 60 minutes). Avidin-biotin complex

was added, incubated at 37°C (30 minutes) and washed. After that, the prepared 3,3',5,5'-Tetramethylbenzidine (TMB) color developing agent was added, incubated at 37°C in dark (30 minutes). Finally, the absorbance was read at 450 nm. The concentration of TNF- $\alpha$  was expressed as picogram per milligram tissue protein (pg/mg protein).

#### **Transforming growth factor- beta 1 (TGF- $\beta$ 1)<sup>[35]</sup>**

In myocardial homogenate, analysis of TGF- $\beta$ 1 was performed based on the manufacturer's protocol (ELISA Kit, MyBioSource, San Diego, California, USA). The sample was added into each well, washed, and biotinylated anti-rat was added and incubated at 37°C for 60 minutes. After washing, the TMB color developing agent was added and incubated at 37°C in dark (30 minutes). The absorbance was read at 450nm and the concentration was expressed as picogram per milligram tissue protein (pg/mg protein).

#### **Histological studies**

The heart apices from the left halves, which represented mostly the left ventricle myocardium, were divided into two parts, one part was preserved in 10% formol saline then processed to obtain (5-6  $\mu$ m) thin sections from paraffin blocks. Sections were routinely stained with hematoxylin and eosin (H&E) and Masson's Trichrome for light microscopic examination<sup>[36]</sup> using (Olympus BX41, Tokyo, Japan) equipped with digital camera (Olympus DP20, Tokyo, Japan) at the CERRMA, Faculty of Medicine, Alexandria University.

The other part was cut into smaller pieces (~1 mm<sup>3</sup>) and immediately fixed in 3% phosphate buffered glutaraldehyde pH 7.4. Then, tissue samples were processed into ultrathin sections, mounted on copper grids, and examined and photographed by the transmission electron microscope (TEM) (JEM-1400 plus, Tokyo, Japan)<sup>[37]</sup> at the Electron Microscope Unit in the Faculty of Science, Alexandria University.

#### **Immunohistochemistry staining with anti-caspase 3<sup>[38]</sup>**

Immunohistochemical staining with anti-caspase-3 was performed. The poly-L-lysine-coated slides were deparaffinized, rehydrated and rinsed in Tris-buffered saline (TBS; pH 7.4). The endogenous peroxidase activity was inactivated with 3% hydrogen peroxide. Then, incubated with the primary antibody rabbit polyclonal anti-caspase-3 (1:1000 dilution, Cell signaling technology, Danvers, USA, catalog number # 9662). Next, incubated with the secondary antibody: anti-rabbit horseradish peroxidase (HRP). Diaminobenzidine (DAB) chromogen was added to visualize the immune reaction. Positive (tonsils) and negative controls were included. The positive reaction appeared as brown in color.

#### **Histomorphometry**

Histomorphometry was performed, using NIH Fiji program (NIH, Bethesda, MD, USA). The area

percentage of collagen fibers in Masson's trichrome stained sections and positive reaction to anti-caspase-3 of immunohistochemistry sections were estimated in five randomly selected sections, from images captured at microscopic magnification of 200 and 100 respectively, in each group. Data was presented as mean  $\pm$  standard deviation (SD).

#### **Statistical analysis<sup>[39]</sup>**

Data were supplied to the computer and analyzed using version 20.0. IBM SPSS software package (Armonk, NY: IBM Corp). To verify the normality of distribution, the Kolmogorov-Smirnov test was used. Quantitative data were described using range (minimum and maximum), mean, standard deviation and median. Significance of the obtained results was judged at the 5% level. The F-test (ANOVA) was used for normally distributed quantitative variables, to compare between more than two groups. The Post Hoc test (Tukey) was used for pairwise comparisons. In addition, the Student t test was used for the normally distributed quantitative variables, to compare between two groups.

## **RESULTS**

### **Characterization of BM-MSCs**

#### **Morphological characterization**

The cell cultures were observed daily using the phase contrast inverted light microscope. At P3 the culture cells were spindle in shape, displaying 60-70% confluency (Figure 1A) and reached 80-90% confluency after 7-9 days exhibiting flattened, fibroblastic like cell monolayer with proliferating cells (Figure 1B,C).

#### **Colony-forming unit-fibroblast (CFU-F) assays**

Cells gradually proliferated into small colonies, which increased after 14 days of culture forming larger colonies clearly detected with crystal violet staining (Figure 1D). The colony-forming assay showed that each well with 100 cells yielded 90%  $\pm$  1.06 of colonies after 14 days.

#### **Immunophenotyping of MSCs by flow cytometry**

Fluorescence-activated cell sorting (FACS) analysis for P3 showed that BM-MSC cultured cells positively co-expressed cluster of differentiation (CD) surface markers CD73, CD105, CD 44 and CD 90 (96.17%, 96.37%, 95.69% and 94.23% respectively). Meanwhile, they were negative for the hematopoietic markers CD11b and CD45 (Figures 2 A-E).

#### **Homing of BM-MSCs**

The labelled BM-MSCs were recognized by their intense red fluorescence, among cardiomyocytes, in the heart sections. (Figure 2 F).

### **Characterization of MSCs-EVs**

#### **Protein content**

The results revealed that the protein concentration

was 1400 mg/ml. This amount was the yield from 5 x 10<sup>6</sup> cultured MSCs.

#### **Transmission electron microscopy (TEM)**

Exosomes appeared as membrane bounded, rounded structures with sizes ranging from 31.44 to 116.00 nm (Figure 3A,B).

#### **Zeta sizing. (Malvern, UK)**

Zeta sizing showed isolated vesicles had a mean size of 160.3 nm and an intensity of 92.6%, suggesting that most of the isolated EVs were of the exosome class (Figure 3C).

#### **Western blot characterization and quantitative analysis**

A key step in EV characterization depends on identifying surface CD markers. Western blot analysis of BM-MSC-vesicles revealed that CD63 and CD81 were highly expressed in the isolated vesicles as compared with the MSCs' samples. Quantitative analysis of the markers' expression revealed their significant increase in the isolated vesicles indicating that the sample was certainly exosomes (Figures 3D,E).

#### **Biochemical results**

##### **Cardiac enzymes**

Cardiac troponin I (cTnI) and Creatine kinase-MB (CK-MB)

The current results showed significant increase in serum levels of cTnI and CK-MB enzymes in the group II (ISO) compared to group I (C). Group III (EXO) and group IV (ST), revealed significant decreased levels of both enzymes as compared to the ISO group II (ISO). In addition, after four weeks both enzymes showed non-significant difference in groups III (EXO), IV (ST) and V (R), as compared to group I (C) (Figures 4 A,B).

##### **Malondialdehyde (MDA)**

A significant rise was observed in group II (ISO) as compared to group I (C). Meanwhile, group III (EXO) showed a significant decrease as compared to groups II (ISO), IV (ST) and V (R). In addition, it was significantly decreased in group IV (ST) as compared to group II (ISO), yet it was significantly increased in comparison to group III (EXO). Furthermore, group V (R) demonstrated significantly increased level as compared to group I (C) and group III (EXO) (Figure 4 C).

##### **Total antioxidant capacity (TAC)**

Cardiac homogenate level of TAC was markedly reduced in group II (ISO) as compared to group I (C). As regards group III (EXO), the TAC was significantly increased as compared to group II (ISO). Group IV (ST) showed significant increase in the TAC as compared to group II (ISO) and was significantly decreased compared to group III (EXO). TAC in group V (R) was significantly decreased as compared to group I (C) (Figure 4 D).

##### **Tumor necrosis factor -alpha (TNF- $\alpha$ )**

Cardiac homogenate TNF-  $\alpha$  level in group II (ISO) was significantly increased as compared to group I (C). Treatment with EXO in group III, resulted in a marked reduction in the level of TNF-  $\alpha$  that was insignificant with group I (C). While treatment with stem cell resulted also in reduction in the level of TNF- $\alpha$ , yet it was still significantly increased as compared to group I (C). The level in R group V was significantly increased as compared to group I (C) (Figure. 4 E).

##### **Transforming growth factor -beta 1 (TGF- $\beta$ 1)**

The levels of TGF-  $\beta$ 1 revealed a significant increase in group II (ISO) as compared to the group I (C). Both groups III (EXO) and IV (ST) revealed significantly decreased levels as compared to group II (ISO), yet the level was still significantly increased in group IV (ST) as compared to group I (C). Furthermore, TGF-  $\beta$ 1 level was significantly increased in group V (R) as compared to group I (C) (Figure 4 F).

#### **Histological results**

##### **Light microscopic results**

###### **H&E-stained sections**

###### **Group I: Control group (C)**

The ventricular myocardium revealed branching and anastomosing muscle fibers, separated by slit-like interstitial spaces with blood capillaries. The muscle fibers depicted eosinophilic sarcoplasm with oval vesicular centrally located nuclei. The fibers appeared formed of cardiomyocytes joined together at the intercalated discs (ICDs) that were identified as deeply stained transverse lines across the fibers (Figures 5 A,B).

###### **Group II: ISO group**

Ventricular myocardium of ISO group II revealed variable degenerative changes. Some muscle fibers demonstrated myocytolysis or appeared with homogeneous paler sarcoplasm. Others showed sarcoplasmic vacuolization and focal areas of hyper eosinophilic sarcoplasm. Additionally, interrupted muscle fibers were seen. Small and deeply stained nuclei were frequently observed, while some appeared peripherally situated. Evident mononuclear cellular infiltration was also observed in the interstitial spaces between the muscle fibers. Moreover, wide interstitial spaces with disarrangement and displacement of the neighboring fibers apart, were observed. (Figures 6 A-C).

###### **Group III: EXO group**

Evident amelioration of the degenerative changes was observed. The ventricular myocardium showed apparently normal muscle fibers separated with narrow interstitial spaces. Most of the muscle fibers restored their normal histological features and exhibited central oval vesicular nuclei. Focal areas of myocytolysis and vascular congestion

were still seen. In addition, some nuclei appeared deeply stained. (Figures 7 A-C)

#### **Group VI: Stem cells (ST) group**

Partial amelioration of the degenerative changes was demonstrated. Most of the muscle fibers exhibited nearly normal features with eosinophilic sarcoplasm. Nevertheless, persistence of some foci of sarcoplasmic vacuolization, myocytolysis and hypereosinophilic sarcoplasm were still encountered. Most of the nuclei appeared small and deeply stained, whereas few nuclei appeared vesicular. Relatively wide interstitial spaces, vascular congestion with mild perivascular cellular infiltration, as well as extravasated red blood corpuscles (RBCs), were observed (Figures 8 A-C).

#### **Group V: Recovery (R) group**

The ventricular myocardium showed distorted architecture, where muscle fibers appeared separated with wide interstitial spaces. Most of the fibers exhibited small deeply stained nuclei. Areas of myocytolysis and fragmentation were frequently observed. Sarcoplasmic vacuolization and hypereosinophilic sarcoplasm with small deeply stained nuclei were detected. Vascular congestion with mild perivascular cellular infiltration was also observed (Figures 9 A-C).

#### **Masson's Trichrome stained sections**

Group I (C) sections revealed normal pattern of scanty green stained collagen fibers in the interstitium between the cardiac muscle fibers. In group II (ISO), only few collagen fibers were observed between the widely separated cardiac muscle fibers. Furthermore, collagen fibers were sparsely observed between the cardiac muscle fibers in group III (EXO). Group IV (ST) showed focal areas of collagen deposition. Finally, group V (R) revealed apparently abundant collagen fibers between the cardiac muscle fibers (Figures 10 A-E).

Morphometric study showed insignificant difference in the area percentage of collagen fibers in group III (EXO) as compared to group I (C). Though, the area percentage of collagen in group IV (ST) was significantly higher than group I (C). Meanwhile, group V (R) demonstrated significant increase in the area percentage of collagen in comparison to group I (C) (Figure 10F).

#### **Immunohistochemical assessment for anti-Caspase-3**

Group I (C) revealed a negative anti-caspase-3 reaction. Apparently increased positive reaction to anti-caspase-3 was observed in the sarcoplasm of the ventricular myocytes of group II (ISO) in the form of brownish color. Group III (EXO) and group IV (ST) exhibited focal areas of positive reaction that was limited to the sarcoplasm of some ventricular myocytes. However, group V (R) showed apparent increase in the brown positive reaction in the sarcoplasm of the ventricular myocytes. (Figures 11 A-E). Morphometric analysis demonstrated a significant increase in the area percentage of the anti-

caspase-3 positive reaction in group II (ISO) as compared to group I (C). Generally, treatment with EXO or ST in groups (III and IV respectively) resulted in a significantly decreased anti-caspase -3 reactivity as compared to group II (ISO). Furthermore, it appears that EXO treatment in group III, the expression of caspase-3 was insignificant as compared to group I (C), while it was significantly decreased as compared to group IV (ST). The ST group IV showed a significant decrease in the expression of caspase-3 as compared to group II (ISO), yet the expression was insignificantly decreased as compared to group I (C). Group V (R) revealed a significant increase as compared to group I (C) (Figure 11F).

#### **Electron microscopic results**

##### **Group I: Control group (C)**

The ventricular cardiomyocytes revealed regularly aligned myofibrils with organized sarcomeres, each bounded by two Z lines. The cardiomyocytes appeared surrounded by an intact sarcolemma and separated with a narrow interstitial space. Each cardiomyocyte exhibited an oval centrally located euchromatic nucleus with prominent nucleolus. The cardiomyocytes revealed abundant elongated intermyofibrillar mitochondria arranged in ordered rows pattern with distinct cristae. The sarcoplasm also depicted Golgi complex and mitochondria accumulated in the perinuclear region. The ICDs between the adjacent cardiomyocytes showed repeated interdigitations and regions of fascia adherents, desmosomes, and gap junction (Figures 12 A-D).

##### **Group II: ISO group**

Cardiomyocytes of ISO group revealed areas of disrupted sarcolemma and/or scalloping. Cardiomyocytes were evidently separated by wide interstitial spaces. Some nuclei appeared irregular and peripherally situated. Moreover, some cardiomyocytes showed focal areas with disorganized intermyofibrillar mitochondria. Large, deformed mitochondria with tendency of fusion of neighboring mitochondria were also noticed. Other cardiomyocytes exhibited interrupted myofibrils, multiple foci of myocytolysis and even complete loss leaving myofibril free areas. Segments of the ICDs were disorganized. ICDs further exhibited less folding or interdigitation. Widening of some areas of the ICD was observed as well (Figures 13 A-D).

##### **Group III: EXO group**

Most of the cardiomyocytes preserved their normal structure with intact regular sarcolemma. Furthermore, the myofibrils were regularly arranged, with well registered sarcomeres distinctly delineated by Z- lines. However, myofibrillar loss was seen in few localized areas that were clearly surrounded by apparently normal myofibrils. Interrupted Z-lines with apparently deranged regular registration of sarcomeres was also observed. Moreover, most of the nuclei were centrally located, elongated and euchromatic. The mitochondria exhibited normal structure,

arranged in rows in between the myofibrils and perinuclear. The ICDs preseeded their normal zigzag-like appearance with evident fascia adherents, desmosomes, and gap junction (Figures 14 A-D).

#### Group VI: Stem cells group (ST)

Partial improvement was recognized in this group. The sarcolemma appeared mostly regular and intact, whereas sarcolemmal scalloping was still observed in some cardiomyocytes. Multiple areas of the sarcoplasm exhibited myocytolysis. Nuclei in some cardiomyocytes appeared euchromatic and irregular in outline. The perinuclear mitochondria were apparently normal and intermyofibrillar mitochondria appeared regularly arranged, yet occasionally enlarged with indistinct cristae. The ICDs revealed fascia adherens, desmosomes and gap junction (Figure 15 A-D).

#### Group V: Recovery group (R)

Persistent degenerative changes and distorted myocardium architecture were observed, where some cardiomyocytes showed marked scalloping of the sarcolemma. Moreover, some cardiomyocytes exhibited focal areas of myofibrillar loss. Others showed disorganized intermyofibrillar mitochondria with electron dense matrix. Some nuclei appeared irregular. Disorganized sarcomeres with an absence of the normal banding were observed focally. The ICDs appeared interrupted and disorganized. Some of the interstitial cells depicted abundant parallel cisternae of rough endoplasmic reticulum associated with evident extracellular collagen deposition, thus suggestive of fibroblasts (Figures 16 A-F).

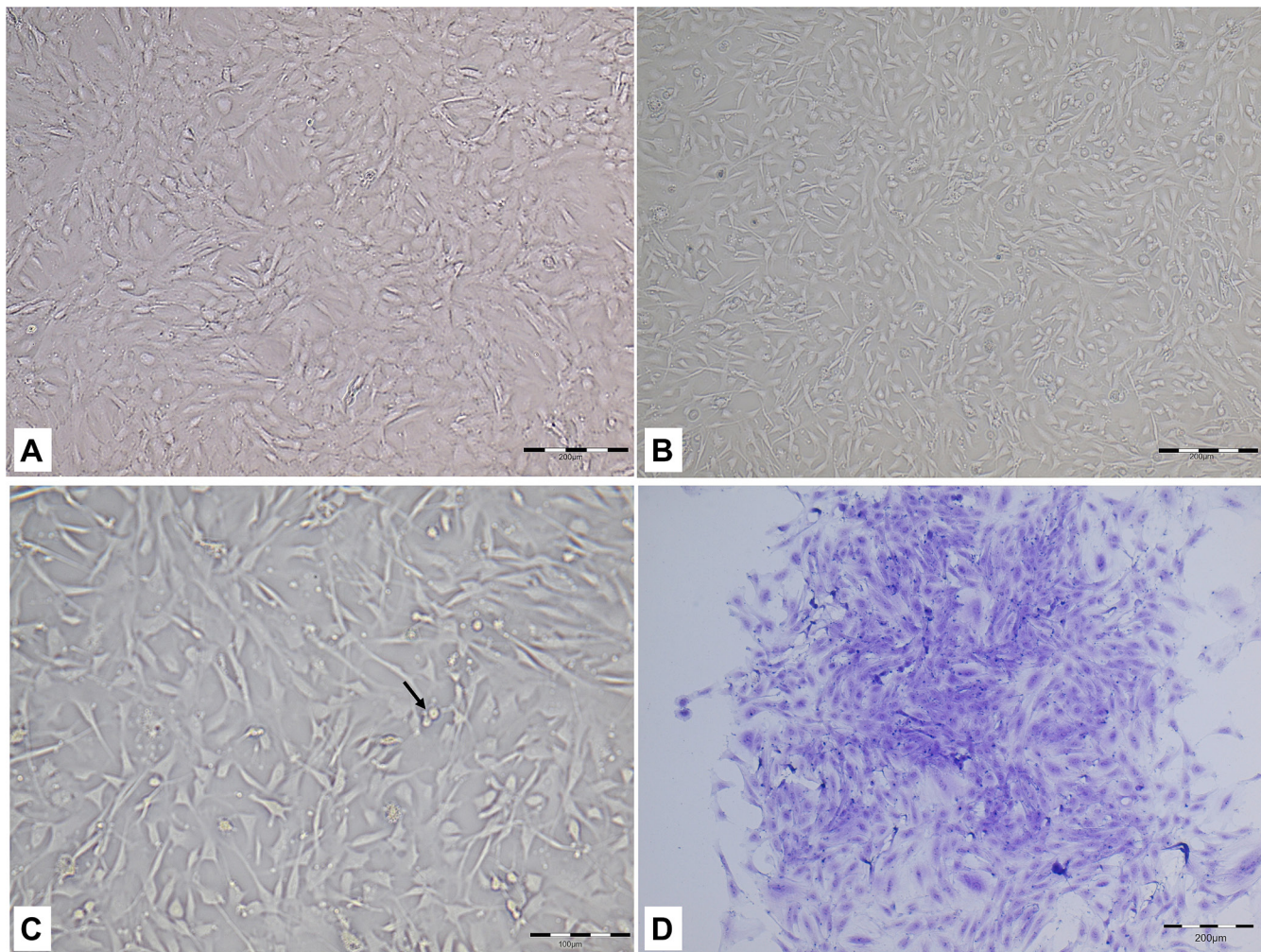


**Fig. 1:** (A-D): Phase contrast inverted microscope pictures of cultured BM-MSCs at P3 showing: A; P3, 60-70 % confluent spindle fibroblast like cells. B; Monolayer 80-90% confluent spindle fibroblast like cells. C; Proliferating cells (arrow). D; Crystal Violet stain showing colony formation. (A, B & D x 100, C x200)

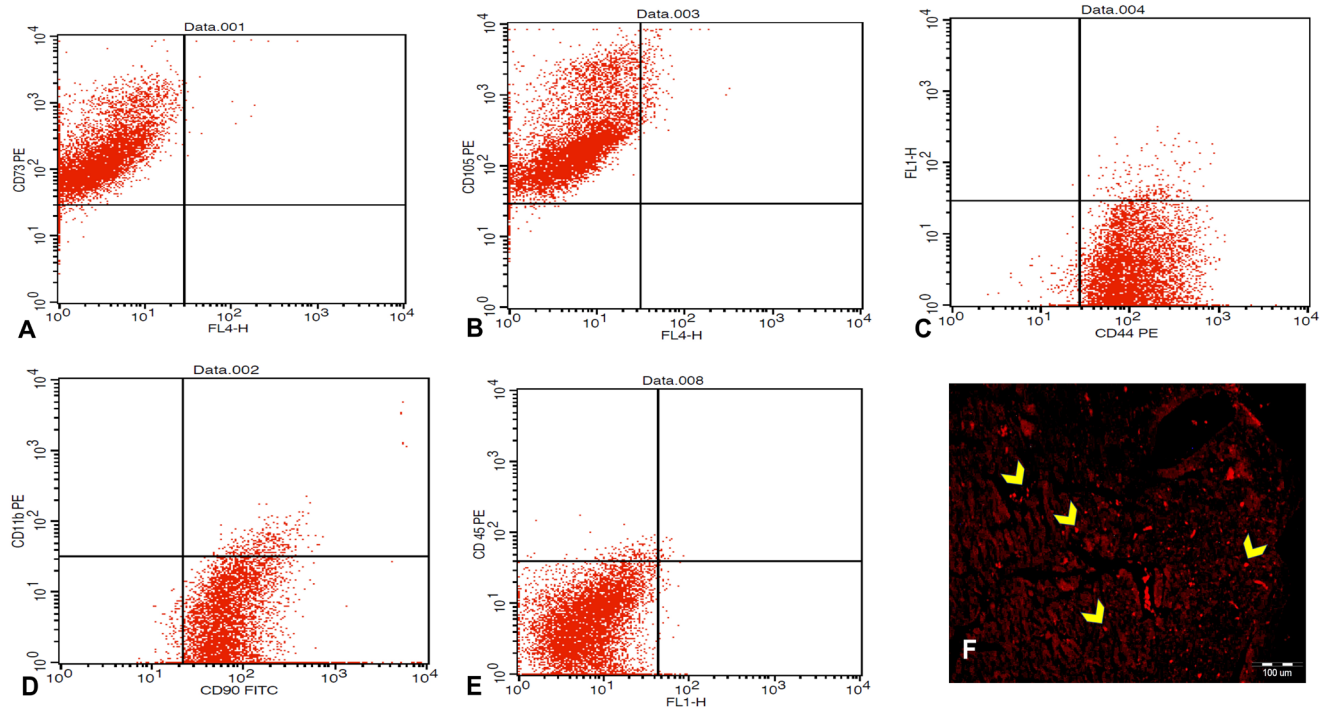


**Fig. 2:** (A-F): A-E; Flow cytometric analysis of the expression of the cell-surface markers of BM-MSCs, A; 96.17% of the cells expresses CD73, B; 96.37% CD 105, C; 95.69% CD 44 and D: 94.23% CD 90. D and E: The cells are negative for the CD 11b and CD45 hematopoietic marker respectively. F; Red fluorescent Dil labeled BM-MSCs (chevron arrows). Fx200.

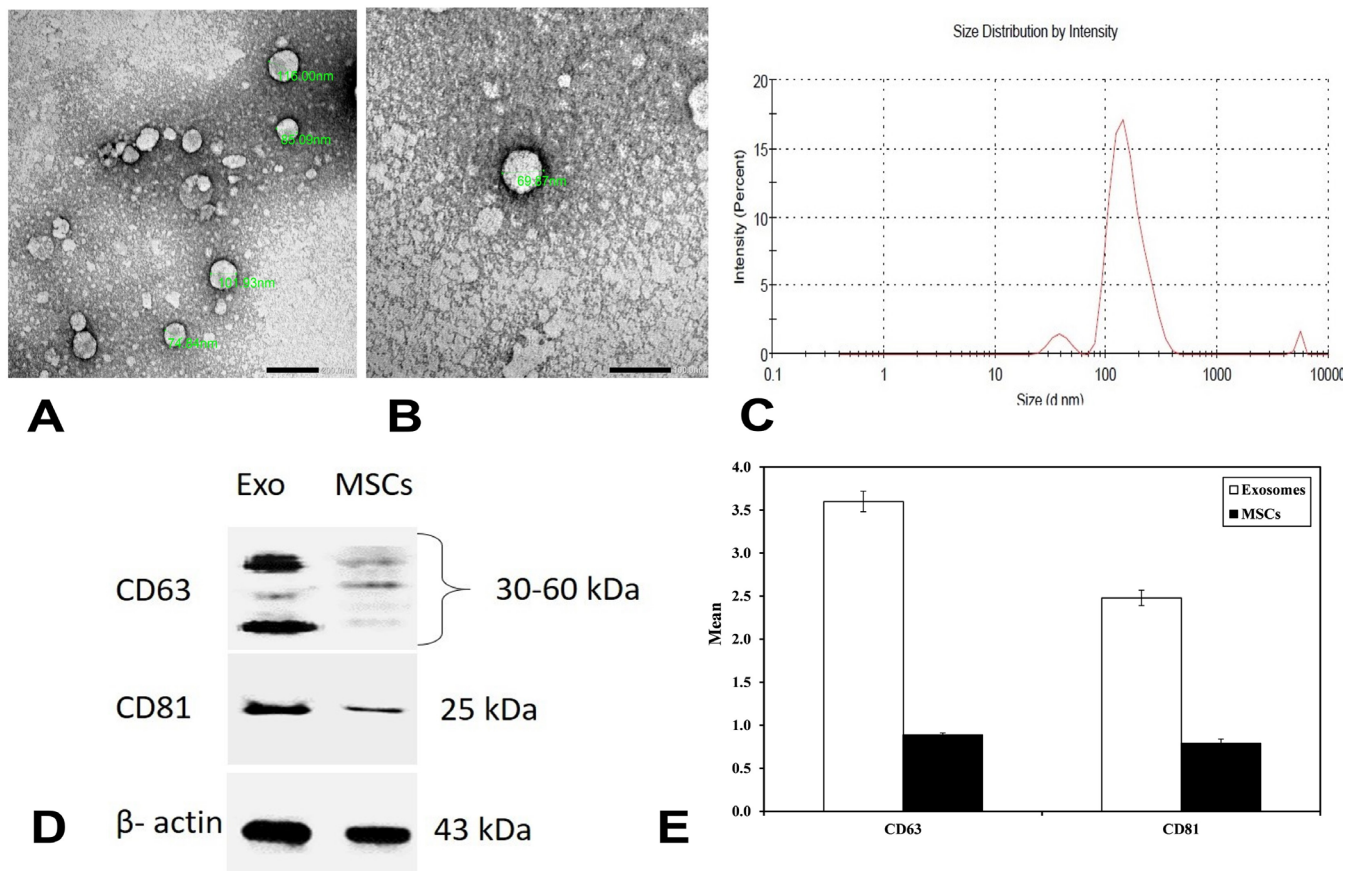


**Fig. 3:** (A-E): Characterization of MSCs-EVs. A; Morphology of EVs by Transmission electron microscope (TEM). B; Higher magnification showing rounded and membrane bounded structures. A x 25000 and B x 60000. C; The size distribution of EVs by Zeta sizer. D; Western blot analysis of CD63 and CD81 surface markers. E; A bar chart representing comparative statistical analysis of the expression of CD63 and CD81 surface markers on the isolated vesicles.

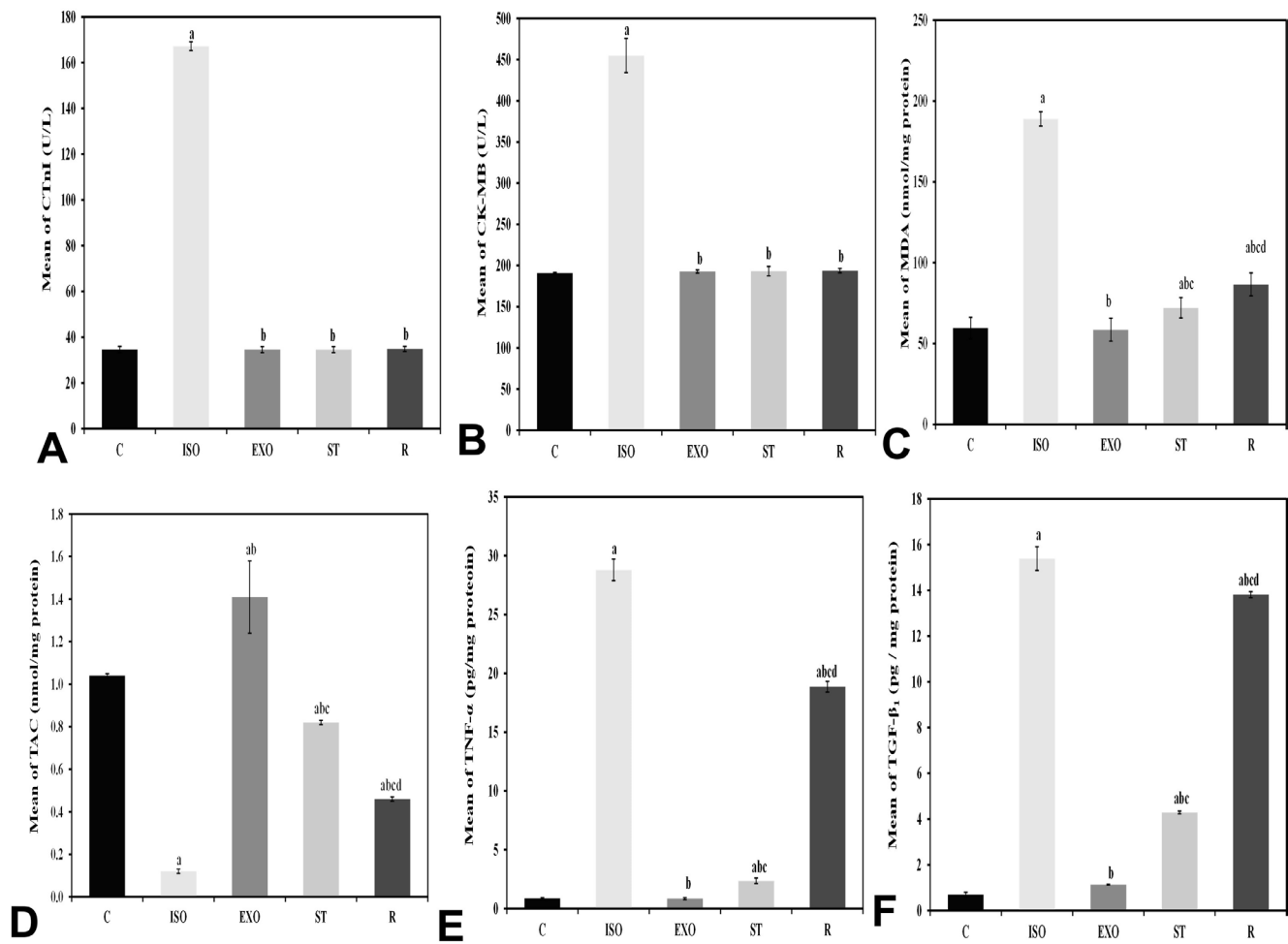


**Fig. 4:** (A-F): Bar charts representing comparative statistical analysis of biochemical parameters. A; Serum cTnI and B; Serum CK-MB levels. C; MDA, D; TAC, E; TNF- $\alpha$ , and F; TGF- $\beta_1$ , in the cardiac homogenates of all the studied groups.

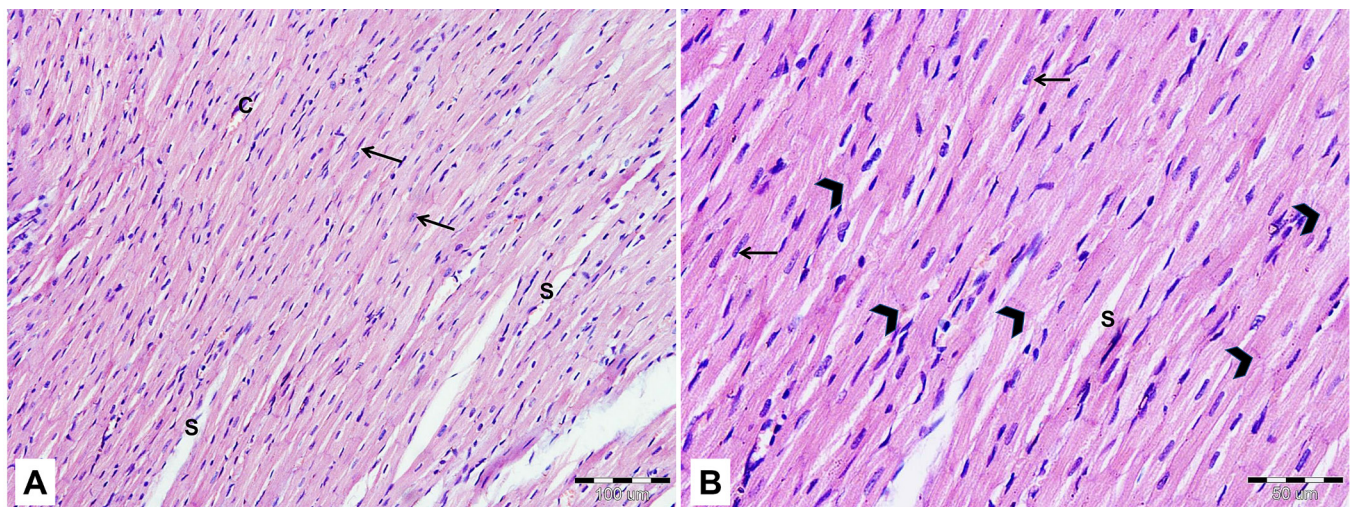


**Fig. 5:** (A & B): Representative light microscopic photomicrographs for the H & E-stained sections group I (C). A and B; Longitudinally cut cardiac muscle fibers with eosinophilic sarcoplasm and central vesicular nuclei (arrows), separated by slit-like interstitial spaces (S). B; Cardiomyocytes are joined at the intercalated discs (chevron arrows). C; blood capillary in A. Mic. Mag. A x 200, B x 400.

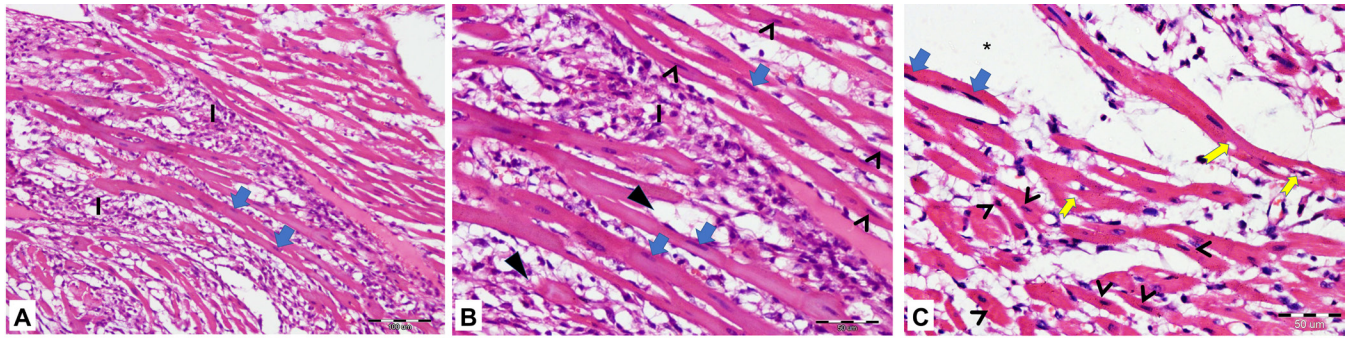


**Fig. 6:** (A-C): Representative light microscopic photographs of the H & E-stained sections of group II (ISO). A; Cardiomyocytes with peripheral deeply stained nuclei (blue arrows) and evident cellular infiltration (I) in between the widely separated muscle fibers are seen. B; (Higher magnification of A) some muscle fibers exhibit deeply stained nuclei and hyper-eosinophilic sarcoplasm (black arrowheads) and myocytolysis (triangle arrows). Other cardiomyocytes show homogeneous paler sarcoplasm and deeply stained peripheral nuclei (blue arrows). I; cellular infiltration. C; Interrupted muscle fibers with hyper-eosinophilic sarcoplasm and deeply stained nuclei (black arrowheads). Sarcoplasmic vacuolization (notched yellow arrows) and wide interstitial spaces (\*) are noticed. Blue arrows; deeply stained peripheral nuclei and hyper-eosinophilic sarcoplasm. Mic Mag. A x 200, B & C x 400.

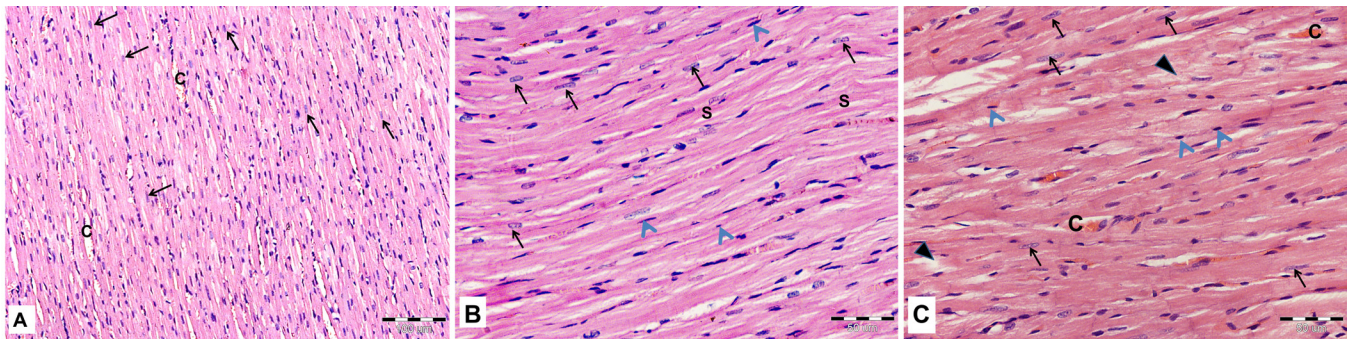


**Fig. 7:** (A-C): Representative light microscopic photographs of the H & E-stained sections of group III (EXO). A; Apparently normal muscle fibers with vesicular central nuclei (black arrows). C; blood capillaries. B & C; Some cardiomyocytes depict vesicular nuclei (black arrows); others depict deeply stained nuclei (blue arrowheads). S; narrow interstitial space in B. C; Focal areas of myocytolysis (triangle arrows) and vascular congestion (C) are noticed. Mic. Mag. A x 200, B and C x 400.

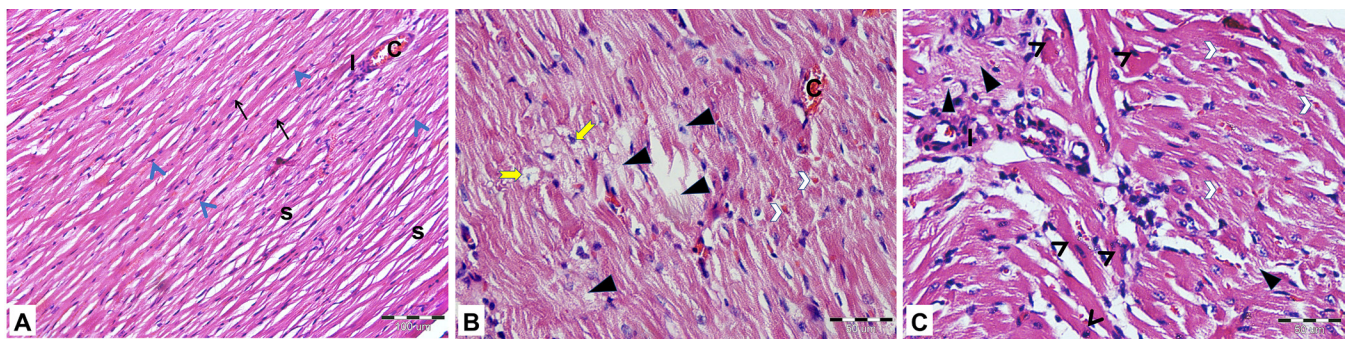


**Fig. 8:** (A-C): Representative Light microscopic photographs of the H&E-stained sections of group IV (ST). A; Longitudinally cut muscle fibers with slightly wide interstitial spaces (S). Small and deeply stained nuclei (blue arrowheads) are noticed, while few appear vesicular (black arrows). C; vascular congestion, I; perivascular cellular infiltration. B; Areas of myocytolysis (triangle arrows) and vacuolization (notched yellow arrows) are seen. White chevron arrows; extravasated RBCs. C; vascular congestion. C; Muscle fibers with hyper-eosinophilic sarcoplasm and deeply stained nuclei (black arrowheads). Perivascular cellular infiltration (I) is also noticed. White chevron arrows; extravasated RBCs, triangle arrows; myocytolysis. Mic. Mag. A x 200, B & C x 400.

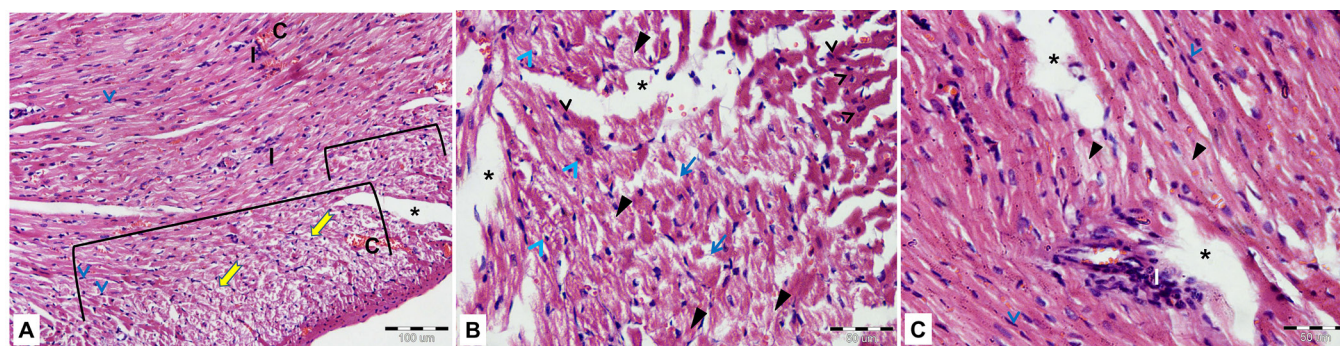


**Fig. 9:** (A-C): Representative light microscopic photographs of the H & E-stained sections of group V (R). A; Wide areas of myocytolysis (brackets), with evident sarcoplasmic vacuolization (notched yellow arrows), deeply stained small nuclei (blue arrowheads) and vascular congestion (C). Wide interstitial space (\*) is noticed. I; perivascular cellular infiltration. B; Fragmented muscle fibers (blue arrows) with myocytolysis (triangle arrows). Other muscle fibers appear hyper eosinophilic with small deeply stained nuclei (black arrowheads). Blue arrowheads; small deeply stained nuclei, (\*); wide interstitial space. C; Perivascular cellular infiltration (I) and wide interstitial spaces (\*) are noticed. Some muscle fibers depict deeply stained nuclei (blue arrowheads) and myocytolysis (triangle arrows). Mic Mag A x 200, B and C x 400.

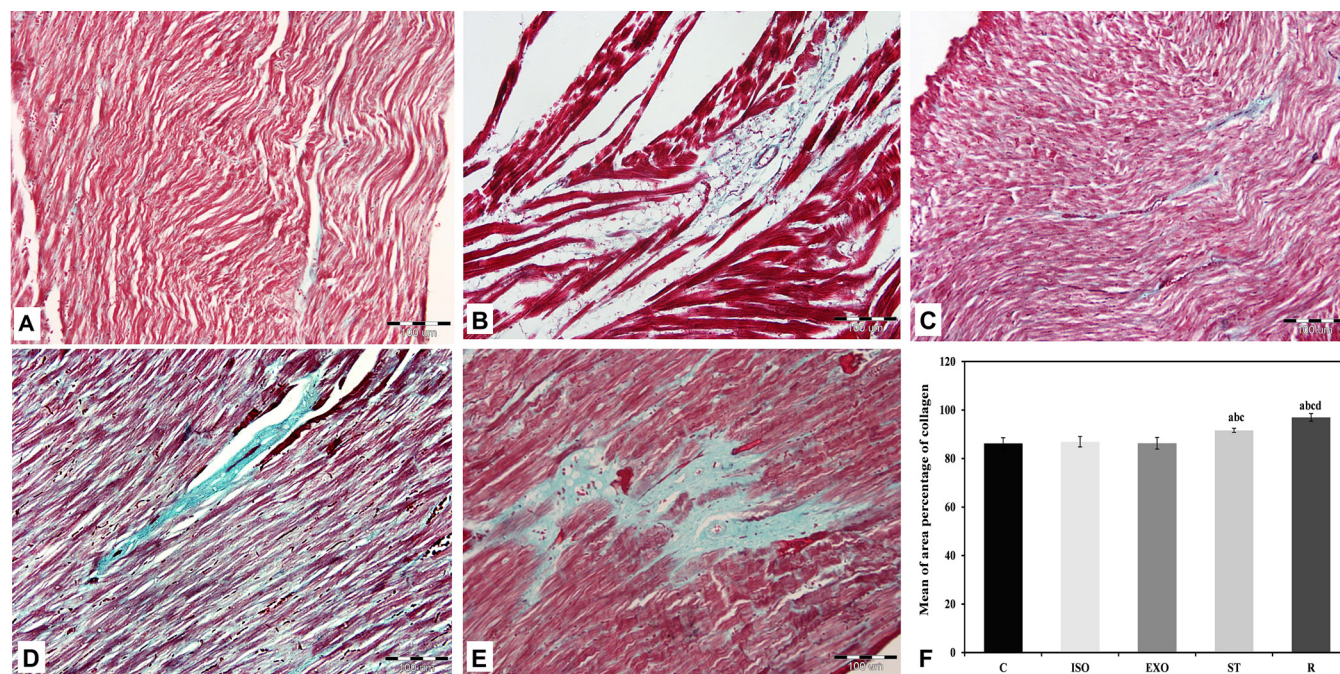


**Fig. 10:** (A-E) Representative light microscopic photographs of Masson's Trichrome stained sections. A (Control group I); normal distribution of collagen fibers in between the cardiac muscle fibers. B (ISO group II); minimal collagen fibers in between the widely separated muscle fibers. C (EXO group III); sparse distribution of collagen fibers. D (ST group IV); focal areas of collagen deposition. E (R group V); Apparently abundant collagen fibers between the muscle fibers. Mic. Mag. A-E x200. F; A bar chart representing comparative morphometric statistical analysis between the studied groups according to the area percentage of collagen.

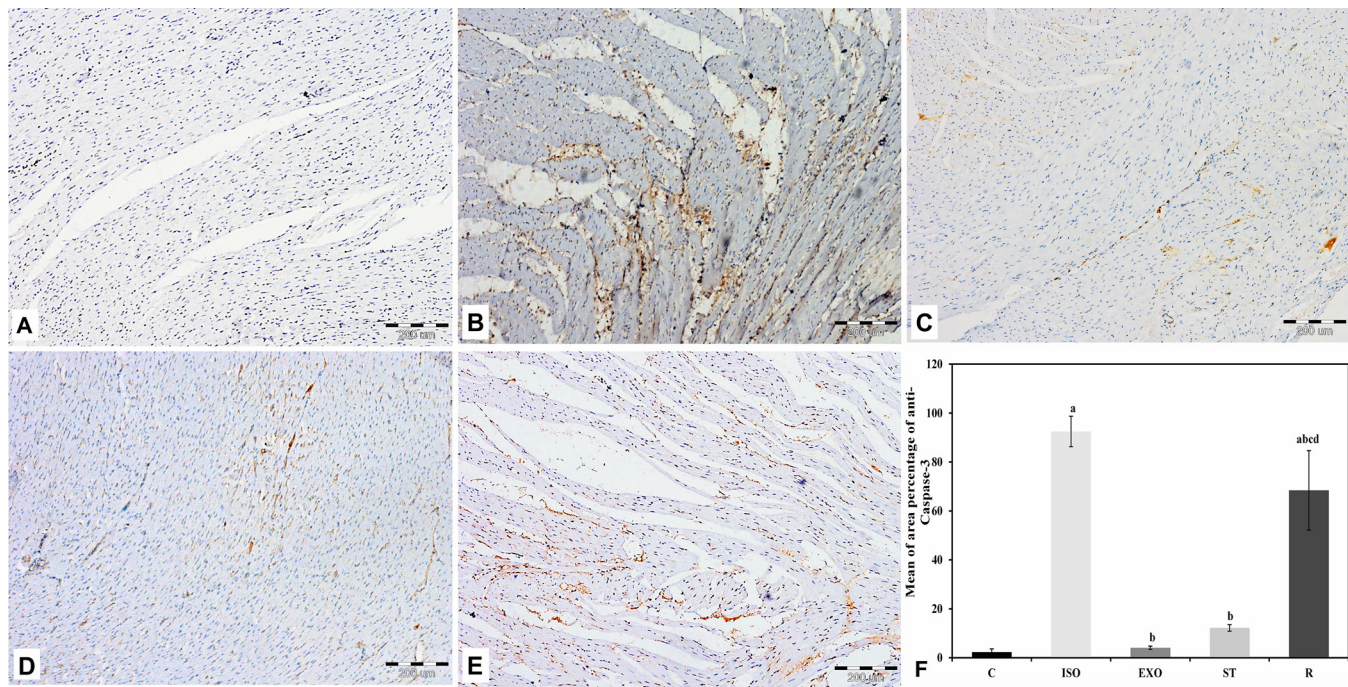


**Fig. 11:** (A-E): Representative light microscopic photographs of the anti -caspase-3 immunohistochemically stained sections. A; Negative immunoreactivity in the control group I. B; apparently increased positive reaction is detected in the group II (ISO). The reaction is observed in the sarcoplasm of the cardiomyocytes. C; Group III (EXO), showing focal sarcoplasmic brown areas of positive reaction. D; Group IV (ST) revealing some areas with positive sarcoplasmic immune reaction. E; R group V showing several areas of positive immunoreactivity mainly sarcoplasmic. F; A bar chart demonstrating a comparative morphometric statistical analysis of the studied groups according to the area percentage of positive reaction to anti-caspase -3. (A-E: Mic Mag. x100).

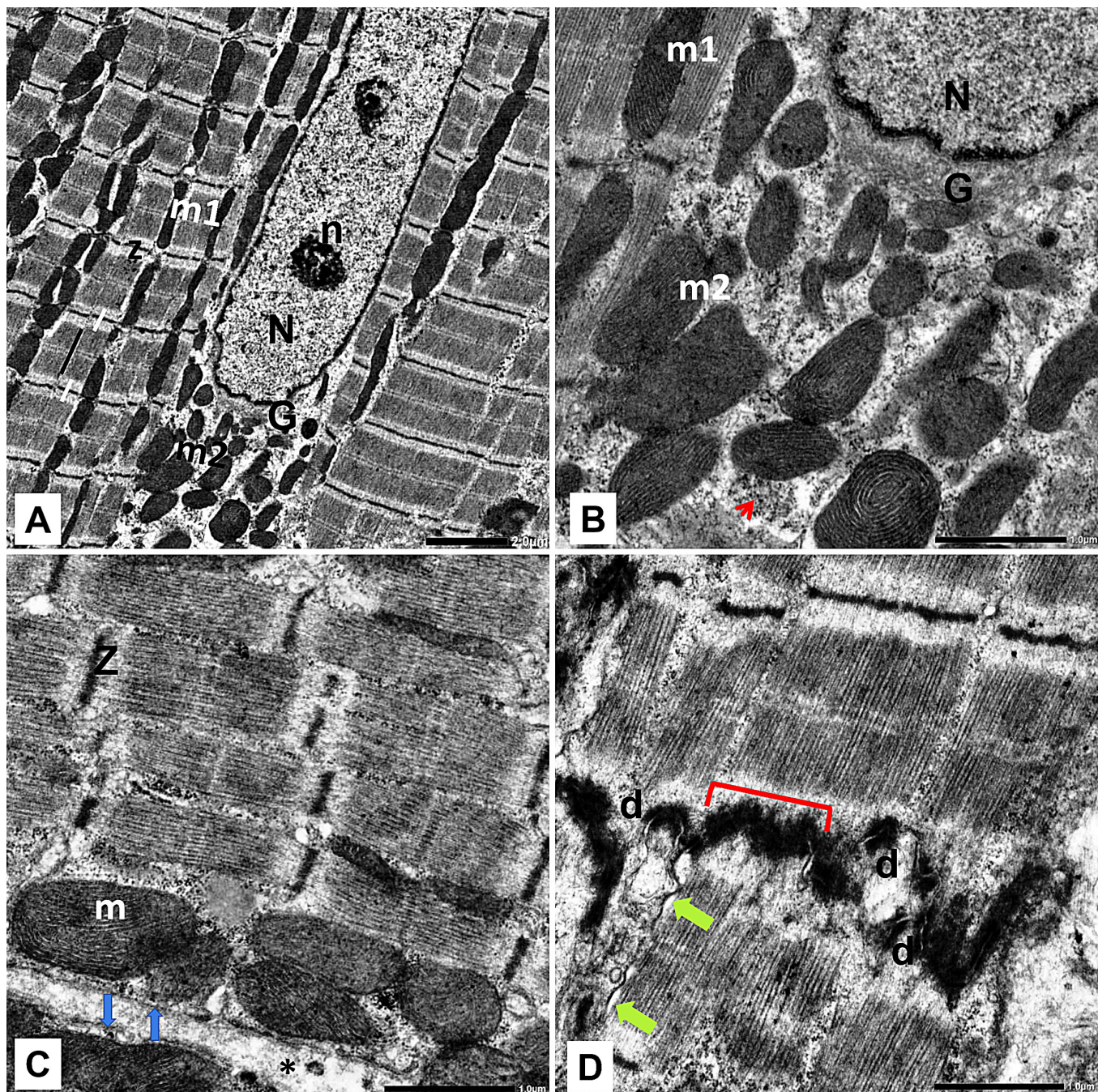


**Fig. 12:** (A-D): Representative TEM photomicrographs of the Control group I. A; Part of a cardiomyocyte with a central elongated euchromatic nucleus (N) and prominent nucleolus (n). The myofibrils show normal banding pattern with alternating dark (black line) and light (white line) bands and evident Z-lines (Z). m1; intermyofibrillar mitochondria. m2; perinuclear mitochondria. B; Perinuclear sarcoplasm showing Golgi complex (G), glycogen granules (red arrowhead) and mitochondria (m1 and m2 exhibiting distinct cristae). C; Parts of two adjacent cardiomyocytes with intact straight sarcolemma (blue arrows). m; mitochondria with distinct cristae, Z; z-line, (\*); Interstitial space. D; Parts of the ICD are seen, fascia adherens (red bracket), desmosomes (d) and the gap junction (green arrows). A x 2500, B, C and D x 8000.

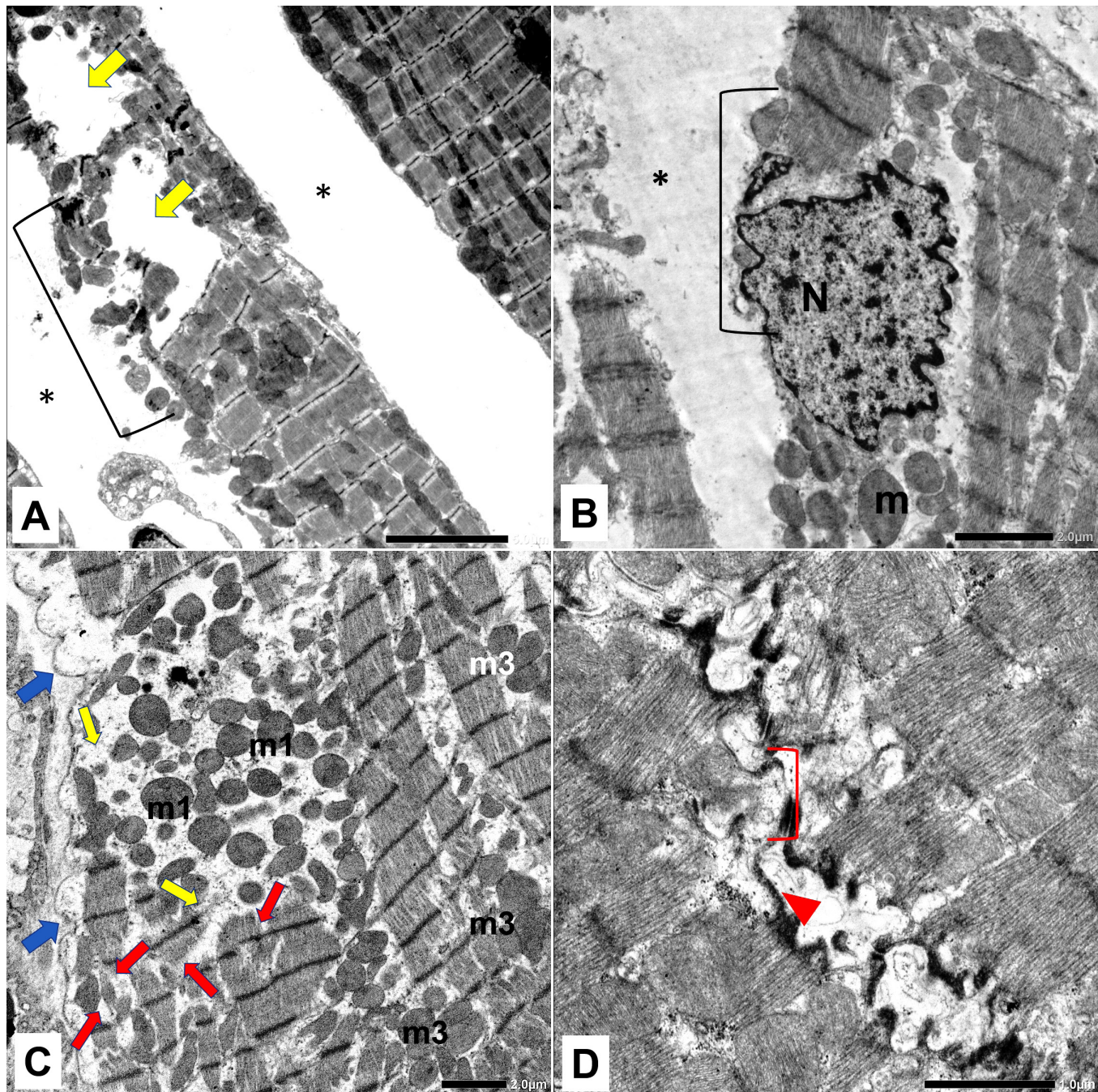


**Fig. 13:** (A-D): Representative TEM photomicrographs of group II (ISO). A; Wide interstitial space (\*), interrupted sarcolemma (bracket) and focal areas of myocytolysis (yellow arrows) are observed. B; Interrupted sarcolemma (bracket), peripheral irregular nucleus (N) and mitochondria (m) with indistinct cristae are seen. (\*) wide interstitial space. C; A cardiomyocyte showing scalloping of the sarcolemma (blue arrows). Areas of myocytolysis (yellow arrows) and focal areas of myofibrillar interruption (red arrows) are observed. Disarrangement of the intermyofibrillar mitochondria (m1) with indistinct cristae and other fused mitochondria (m3) are noticed. D; An ICD with widely separated transverse portion (red arrowhead). Red bracket; Interrupted part of the ICD. Mic. Mag. A x1500, B x2000, C x 2000, D x 8000.

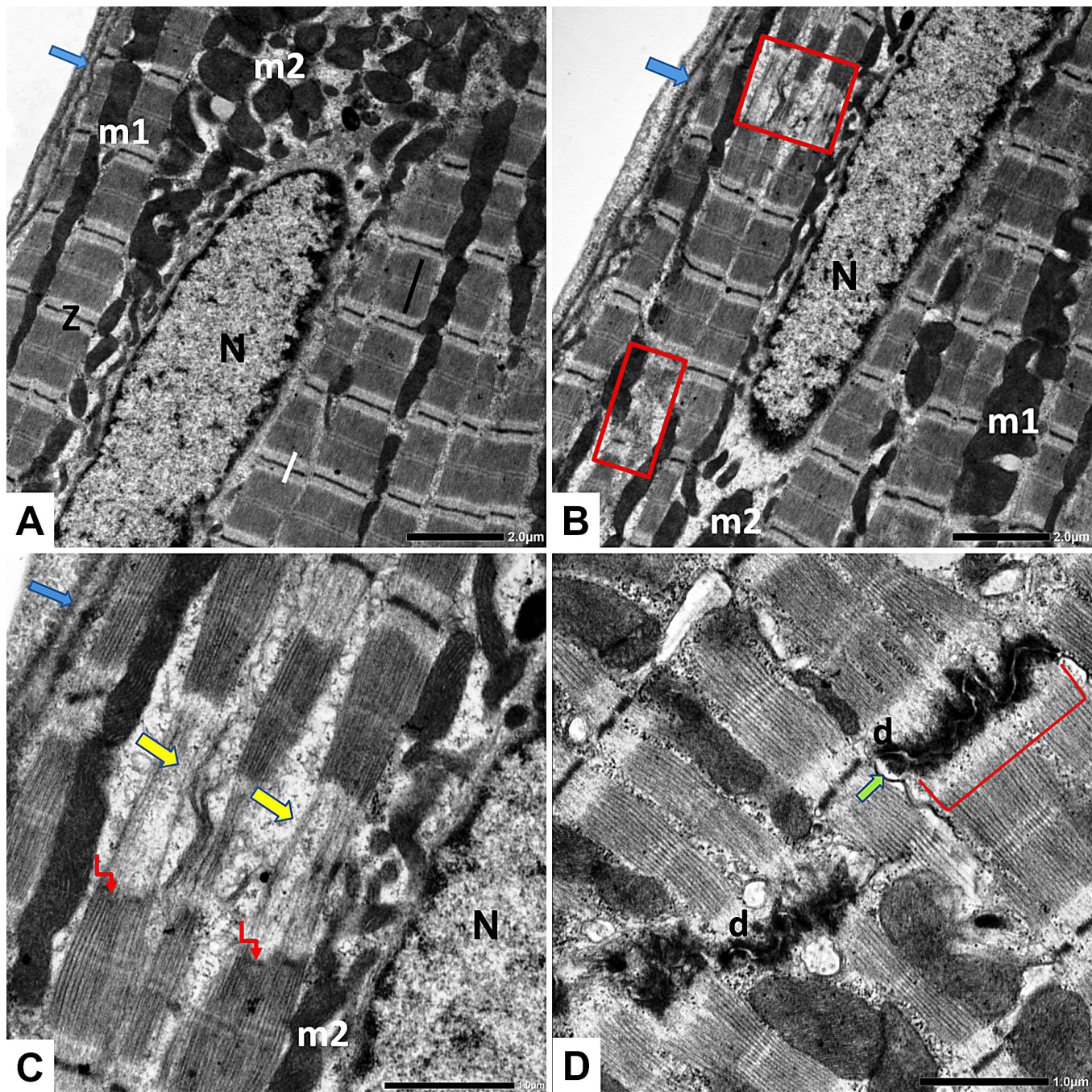


**Fig. 14:** (A-D): Representative TEM photomicrographs of group III (EXO). A; Part of a cardiomyocyte with intact regular sarcolemma (blue arrow), regularly arranged intermyofibrillar mitochondria (m1), perinuclear mitochondria (m2) and normal banding pattern, A band (black line), I band (white line). N; central euchromatic nucleus. Z; Z-line. B & C; Focal areas of myofibrillar loss are noticed (red rectangles) that are evident at a higher magnification in (C) at the yellow arrows. Blue arrow; Regular sarcolemma. N; euchromatic regular nucleus. B; Few intermyofibrillar mitochondria (m1) appear deformed. m2, perinuclear mitochondria. C; Notice the interrupted Z-lines (red elbow arrows). D; An intact ICD with evident fascia adherens (red bracket), desmosomes (d), and gap junction (green arrow). Mic. Mag. A & B x 3000, C & D x 8000

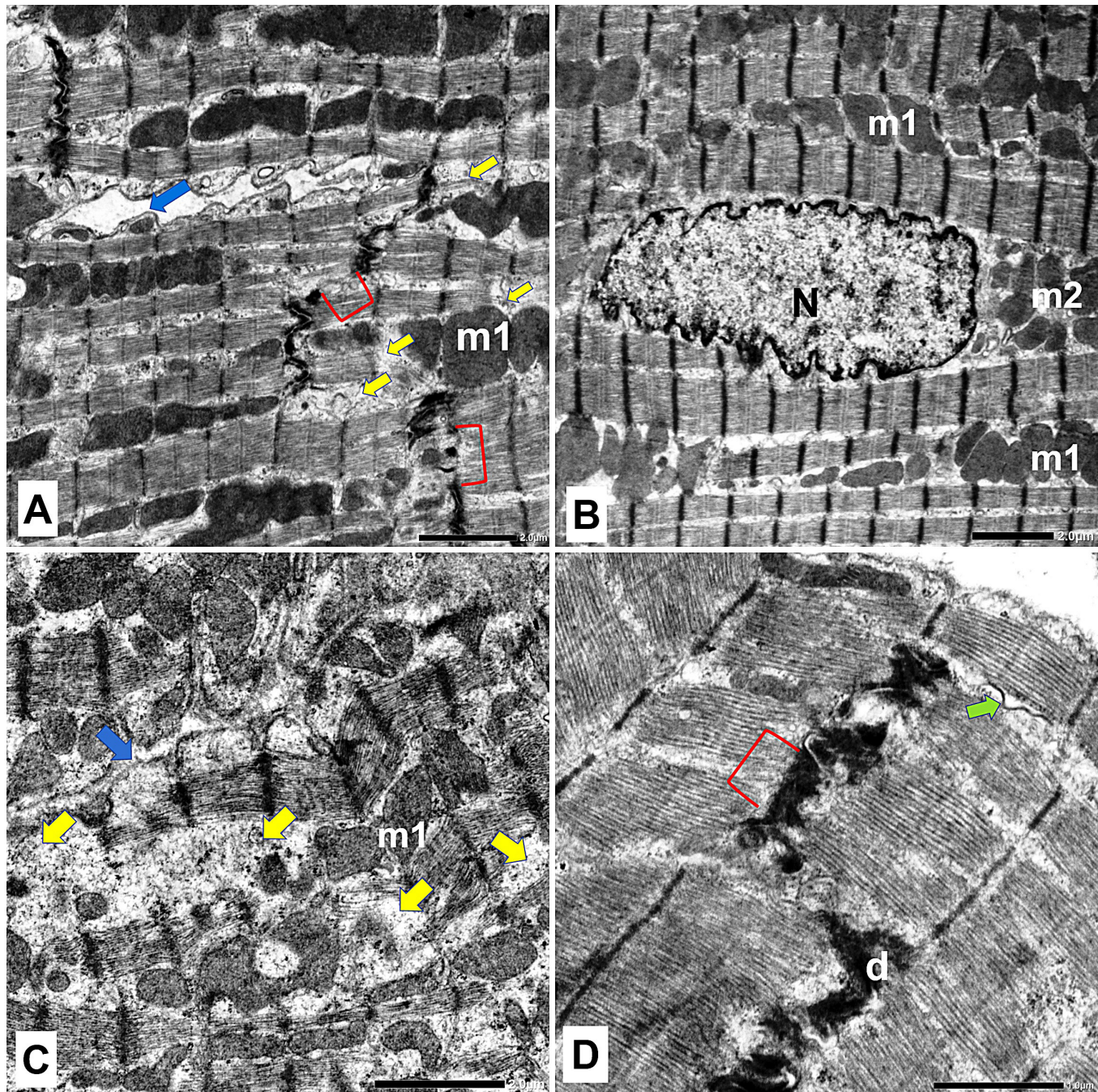


**Fig. 15** (A-D): Representative TEM photomicrographs of group IV (ST). A; Parts of two adjacent cardiomyocytes with scalloped sarcolemma (blue arrow). Some intermyofibrillar mitochondria are enlarged with indistinct cristae (m1). Focal areas of myocytolysis (yellow arrows). Focal areas of interrupted ICD (red brackets) are also seen B; Part of a cardiomyocyte showing central euchromatic nucleus (N) with irregular outline and apparently normal perinuclear mitochondria (m2). m1; regularly arranged intermyofibrillar mitochondria. C; Parts of two adjacent cardiomyocytes with mild scalloping of the sarcolemma (blue arrow) and areas of myocytolysis (yellow arrows). m1; disorganized intermyofibrillar mitochondria with indistinct cristae. D; An ICD revealing fascia adherens (red bracket), (d) desmosome and gap junction (green arrow). Mic. Mag. Ax 3000, B x2500, C x 4000 and D x 8000.

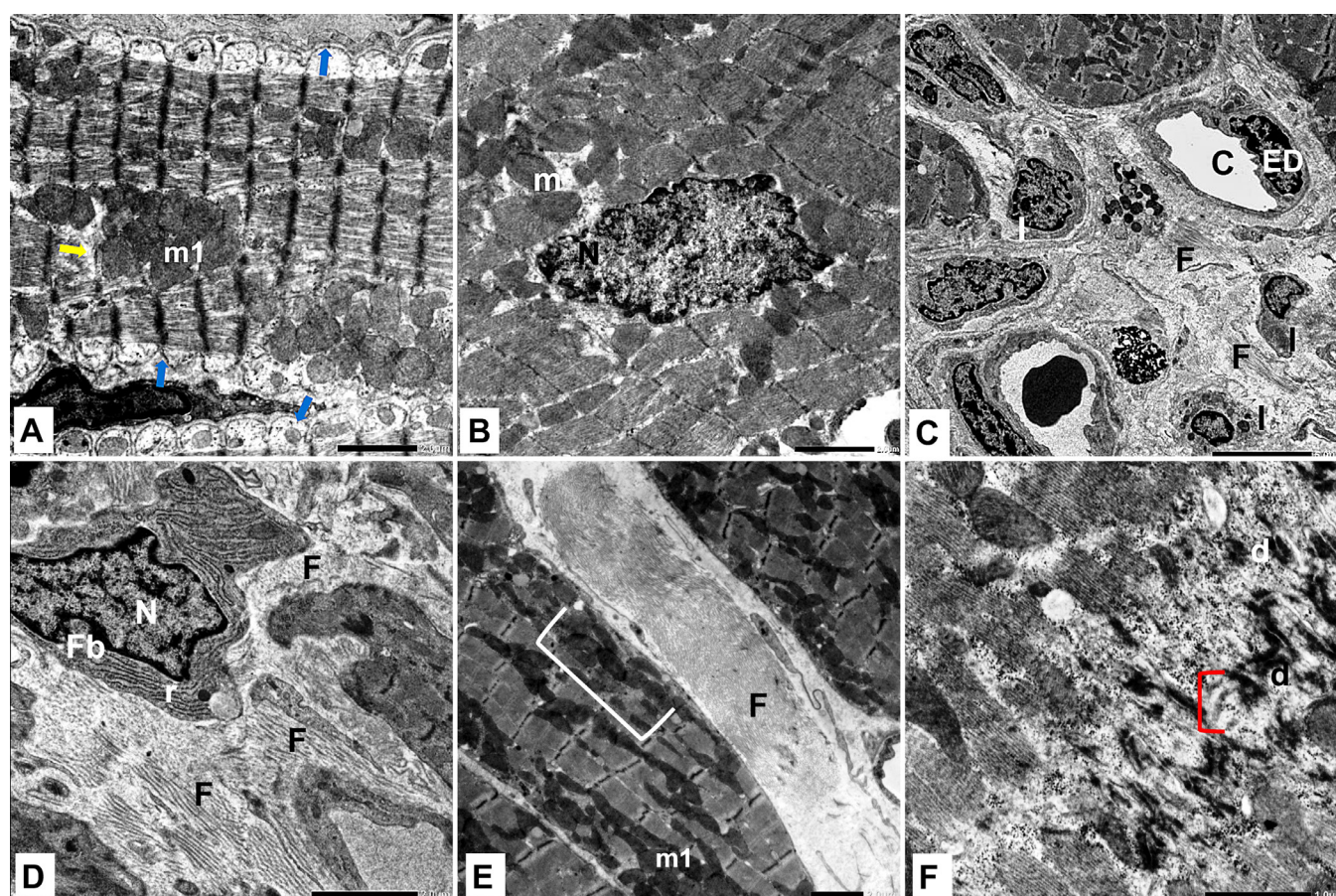


**Fig. 16 (A-F):** Representative TEM photomicrographs of group V (R). A; Scalping of sarcolemma (blue arrows), group of irregularly arranged intermyofibrillar mitochondria with indistinct cristae (m1) and focal areas of interrupted myofibrils (yellow arrow) are seen. B; An irregular nucleus (N) and disorganized intermyofibrillar mitochondria (m1) with indistinct cristae are seen. C; Mononuclear cellular infiltration (I), F; collagen fibrils, C; blood capillary, ED; endothelium. D; One cell shows an euchromatic nucleus (N), cytoplasm with abundant cisternae of rough endoplasmic reticulum (r), suggestive of a fibroblast (Fb) with evident deposition of collagen fibrils (F). E; Abundant collagen fibrils (F) in the interstitium and loss of regular banding (bracket). Mitochondria (m1) appear disarranged with indistinct cristae. F; An interrupted ICD (red bracket), d; desmosomes. Mic Mag A & B x 3000, C x 1500, D x 4000, E x 2000, F x 8000.

## DISCUSSION

Myocardial infarction is considered as a major, worldwide health problem with serious impact on myocardial function and accompanied with high rates of morbidity and mortality. However, recent evolution in the field of regenerative medicine, that targets regeneration of the cardiomyocytes, has emerged. Herein, BM-MSCs and their derived exosomes have attracted much attention recently, as a novel therapeutic modality aiming to restore the functional capacity of the myocardium through enhancement of the regenerative process.

In such a context, the current study aimed to investigate histologically and biochemically the therapeutic potential of EXO secreted by BM-MSCs in ISO induced myocardial changes in a rat model, in comparison to BM-MSCs.

Occurrence of myocardial injury in ISO group was confirmed biochemically through significantly elevated serum levels of cTnI and CK-MB as compared to group I (C) and was furthermore established by the histological results. This can be referred to deranged integrity of cardiomyocytes membrane, as well as myocytolysis

with subsequent releases of endogenous enzymes. CK-MB is one of the isoenzymes of CK and is regarded as a myocardium specific enzyme, thus it was the enzyme of choice in the present study to assess acute myocardial injury. Its serum level increases within six to twenty four hours following myocardial injury and returns to normal within two or three days<sup>[40]</sup>.

Myocardium cTn-I is a specific marker where it bound to troponin T. In a study by Starnberg *et al*<sup>[41]</sup>, it was documented that serum level of cTn-I reaches a peak within twenty four hours post myocardial injury and returns to its basal level within fifty four hours due to its relatively fast clearance.

Histologically, variable oxidative stress induced degenerative changes were observed in H & E stained sections within myocardium of ISO group, where cardiomyocytes depicted myocytolysis, cytoplasmic vacuolization, hypereosinophilic sarcoplasm and small dark nuclei.

ISO is a strong synthetic catecholamine that induces MI through the interplay of several factors, which eventually

induce a state of stress within the myocardium. ISO in large doses overstimulates beta-adrenergic receptors, hence inducing increased heart rate, myocardial contraction, together with hypotension. Thereby, increased oxygen consumption is required by the myocardium, but cannot be fulfilled due to the induced hypotension, thus inducing hypoxia. Such a hypoxic state leads to coagulative necrosis of cardiomyocytes that is demonstrated in the present study by focal areas of hyperesinophilia in cardiomyocytes. Moreover, ISO induces a state of oxidative stress, which has a significant role in induction of myocardial injury<sup>[42,43]</sup>.

ISO undergoes auto-oxidation, where its hydroxyl group is oxidized with subsequent formation of quinines that react with oxygen and produce excessive cytotoxic reactive oxygen species (ROS). Accordingly, a state of imbalance between ROS and endogenous antioxidants is encountered. Consequently, peroxidation of membrane polyunsaturated fatty acids occurs resulting in altered cell membrane structure and derangement of transport across the cell membrane. Malondialdehyde (MDA) is produced as a biproduct of membrane lipid peroxidation, and it is implicated in enzymatic inactivation, together with myocardial membrane damage that occurs along with oxidative stress. Moreover, it aggravates the oxidative stress through either release of more ROS or decreasing endogenous antioxidant capacity condition. Additionally, mitochondrial membrane structural integrity is affected together with altered mitochondrial enzymes activity, thus decreasing mitochondrial capacity for generation of endogenous antioxidant enzymes, together with increased release of ROS from the mitochondria. As a result, oxidative stress is further accentuated within the myocardium<sup>[42,44,45]</sup>. In the present study, oxidative stress was confirmed biochemically, where MDA level was significantly increased within the myocardium in rats of group II (ISO) as compared to group I (C). Herein, MDA is considered as a reliable oxidative stress marker early, where its level peaks within 48 hours post infarction, followed by a gradual decline overtime within the tissue. As such, MDA level in groups III (EXO), IV (ST) and V (R) was significantly reduced as compared to group II (ISO).

Meanwhile, decreased level of TAC in the tissue was demonstrated in group II (ISO) as compared to group I (C), thus reflecting overwhelmed endogenous antioxidant capacity<sup>[42,46]</sup>. However, increased level of TAC was encountered in different treatment and recovery groups, thus denoting a compensatory mechanism by the cardiomyocytes to restore the redox balance. Our results came in agreement with a study performed by Dizaji *et al.*<sup>[46]</sup>. Notably, the antioxidant effect of BM-MSCs and EXO was supported, where TAC levels demonstrated significant increase in group III (EXO) and group IV (ST) as compared to group V (R), with group III (EXO) revealing a significant increase in comparison to group IV (ST).

Moreover, the hypoxia associated with MI aggravates mitochondrial dysfunction, where electron transport

chain is deranged with subsequent accumulation of toxic metabolites, diminished amount of adenosine triphosphate, and excessive calcium load within cardiomyocytes. Eventually, mitochondrial enzymes implicated in the respiratory chain and oxidative phosphorylation is affected with subsequent decreased energy production, thus aggravating myocardial damage. Consequently, activity of Na<sup>+</sup>/K<sup>+</sup> ATPase is reduced with subsequent derangement of Na<sup>+</sup> transport, thus explaining the encountered sarcoplasmic vacuolization<sup>[47,48]</sup>.

Electron microscopic results were consistent with the light microscopic and the biochemical results. In this context, variable oxidative stress induced degenerative changes were observed in group II (ISO), such as, scalloping or interruption of sarcolemma, cytoplasmic vacuolization, and irregular nuclei. Moreover, mitochondria appeared abnormally enlarged and disarranged. Mitochondrial changes can be explained on basis of ROS induced derangement of mitochondrial membrane structural integrity and mitochondrial enzymatic function. Subsequently, mitochondrial production of ATP is decreased with subsequent accentuation of energy depletion within the myocardium. As such, mitochondria undergo compensatory increase in size or fusion of neighboring mitochondria, which was observed in the present study<sup>[49]</sup>.

Another interesting result observed was the evident anti-caspase 3 positive reaction in the group II (ISO). The reaction was markedly reduced after EXO treatment rather than BM-MSCs treatment that showed less reduction in the anti-caspase 3 reactivity. This was documented immunohistochemically and its quantitative analysis.

Here it must be emphasized that apoptosis is implicated, as well, in the induced myocardial damage by ISO, where oxidative stress enhances expression of the proapoptotic proteins Bcl-2 associated X protein (Bax) and Bcl-2 homologous antagonist/killer (BAK) family in the mitochondrial membrane, thus overwhelming the antiapoptotic effect of B-cell lymphoma 2 (Bcl-2). Therefore, cytochrome c is released from the mitochondria that ultimately ends with activation of caspase-3. Subsequently, poly ADP ribose polymerase (PARP), an enzyme that has a crucial role in repair of DNA and protection against apoptosis, is damaged by the activated caspase-3. This eventually leads to activation of caspase cascade that induces structural damage to the cytoskeleton<sup>[47]</sup>. This was consistent with the ultrastructural changes encountered in the intercalated discs, where disintegration of intercalated discs components was observed in group II (ISO). Moreover, chromatin fragmentation occurs during apoptosis, together with direct impact of ROS on DNA, thus the nuclear changes encountered in group II (ISO) are explained. Furthermore, lysosomal membrane stability is disrupted because of membrane lipid peroxidation, hence contributing to the induced apoptosis and inflammation through release of lysosomal enzymes. In addition, lysosomal hydrolases activity is enhanced, thus contributing to myocardial damage<sup>[42]</sup>.

In the current study, mesenchymal stem cells derived exosomes were preferred regarding feasible isolation from culture medium of BM-MSCs. Isolation of exosomes is a challenging issue, however, the protocol adopted in the current study was ultracentrifugation. Such a protocol was in line with previous research work that demonstrated satisfactory outcome<sup>[50,51]</sup>.

Successful isolation of the target EXO was confirmed through morphological characterization by transmission electron microscope examination, where membrane bounded vesicles ranging in size between 31.44 to 116.00 nm were observed. In addition, zeta analyzer revealed size of 160.3 nm. The current results were in agreement with Zhang *et al*<sup>[16]</sup>, who mentioned that EXO range in size between 30-200 nm in diameter. This was further confirmed by the western blot assay results that demonstrated expression of CD63 and CD81 specific surface markers. These results came in agreement with a previous research work<sup>[52]</sup>.

As regards the therapeutic potential of BM-MSCs in MI, there is a growing body of evidence in literature that is mainly due to a paracrine effect mediated through release of variable factors, such as growth factors and cytokines. EXO convey the therapeutic potential of cells of origin in an enhanced pattern, where they contain all such factors. Additionally, their content of variable types of miRNAs, allow them to induce cardio protection more potently. Subsequently, such factors create a favorable tissue microenvironment that allows the regeneration process and the recovery of the myocardium<sup>[53]</sup>.

Nevertheless, BM-MSCs transplantation-based therapy encloses the disadvantage of unsatisfactory homing and survival rates, which decrease their therapeutic role depending on their differentiation capacity into cardiomyocytes or providing supportive structural tissue framework through its differentiation into fibroblasts. As such, paracrine role of BM-MSCs is considered to be more significant<sup>[54]</sup>.

In this context, isolated EXO are emerging as more promising therapeutic strategy in MI, where they are proved to be biologically stable due to their enclosure by a lipid bilayer with sustained stability, thus can transfer their cargo distantly, while preserving their therapeutic potential<sup>[55]</sup>. In this context, Cheng *et al*<sup>[56]</sup> demonstrated elevated levels of miR-1 and miR-208 in urine of acute MI patients, thus suggesting that miRNAs released from injured cardiomyocytes escape degradation by RNases. In view of the aforementioned data, systemic administration of EXO via tail vein injection was the route of choice in the present study. EXO interact with their target cells either through receptor mediated interaction or internalization, thereby influencing cell response. Such an influence is dependent on the EXO content<sup>[16]</sup>.

Histological examination of group III (EXO) and group IV (ST) revealed evident amelioration of degenerative changes that was more marked in EXO group. Biochemical

and immunohistochemical results were consistent with the histological results.

Herein, such an ameliorative effect can be referred to the paracrine antiapoptotic effect of transplanted BM-MSCs post MI, where the hypoxic microenvironment associated with MI potentiates the release of mi-RNA 22 loaded exosomes. As a consequence, proapoptotic genes expression is downregulated by activation of phosphatidylinositol 3-kinase/serine/threonine kinase (PI3K/Akt) pathway<sup>[57]</sup>. In fact, PI3K/Akt pathway is considered to play a key role in modulating apoptosis within cardiomyocytes, where it is regulated by phosphatase and tensin homolog (PTEN). Such antiapoptotic effect is conveyed via exosomes in an enhanced pattern owing to their content of additional mi-RNAs, such as, mi-RNA 144 that acts on PTEN/PI3K/AKT and mi-RNA-486-5p that suppresses the PTEN pathway, thus activating PI3K/Akt pathway<sup>[58]</sup>. In addition, EXO contain mi-RNA 21 that suppresses expression of proapoptotic genes, such as FasL, within the myocardium through influencing a number of intracellular signaling pathways, such as nuclear factor kappa-light-chain-enhancer of activated B cells (NF- $\kappa$ B) and PTEN/AKT/Bcl-2<sup>[59]</sup>.

Moreover, it was suggested by previous research studies that the antiapoptotic effect of the EXO might be mediated indirectly by amelioration of the induced oxidative stress in MI. Herein, some antioxidants are postulated to be delivered by EXO, thus restoring normal biological processes within the cardiomyocytes such as ATP production, with subsequent alleviation of apoptosis<sup>[60]</sup>.

The immunohistochemical results in our study supported the antiapoptotic effect, where expression of caspase-3 was significantly decreased in EXO and ST groups as compared to group II (ISO). However, group III (EXO) demonstrated more decreased expression.

Moreover, group II (ISO) revealed evident inflammation histologically, as well as biochemically. Histologically, mononuclear cellular infiltration and vascular congestion were evident in group II (ISO). Biochemically, tumor necrosis factor alpha (TNF- $\alpha$ ) was significantly increased in group II (ISO) as compared to group I (C). Meanwhile, notable alleviation of inflammation was observed in groups III (EXO) and IV (ST), being more evident in group III (EXO). As for group V (R), residual inflammatory changes were detected.

Inflammation occurs as a consequence to myocardial injury and ischemia. It is previously mentioned in literature that proinflammatory cytokines, such TNF- $\alpha$  and interleukin-6 (IL-6) are detected within the myocardial tissue following ischemia. Upon exposure to hypoxia, cardiomyocytes and myocardial mononuclear macrophages release TNF- $\alpha$  within the infarct area, hence triggering inflammatory cellular infiltration<sup>[40]</sup>. This came in agreement with a study by Yu *et al*<sup>[61]</sup> that demonstrated release of TNF- $\alpha$  enriched exosomes from cultured cardiomyocytes exposed to hypoxia-inducible factor (HIF)-1 $\alpha$ .

Additionally, deranged lysosomal membrane stability is induced by the produced free radicals with subsequent release of lysosomal glycohydrolases and cathepsins into the cytoplasm and circulation. This leads to enhanced production of inflammatory mediators and aggravation of myocardial injury<sup>[62]</sup>.

In addition, cytokine IL-1  $\alpha$  is released from degenerated cardiomyocytes exposed to hypoxia, which in turn stimulates expression of TNF- $\alpha$ , IL-6 and IL-1 $\beta$  by the cardiomyocytes, hence accentuating the inflammatory status after myocardial ischemia MI [40]. Moreover, TNF- $\alpha$  enhances ROS generation and induction of apoptosis<sup>[46]</sup>. It is worth mentioning that such cytokines are related to the remodeling process following MI, where IL-1 $\beta$  stimulates myofibroblasts to release altered collagen fibrils within the infarct area, consequently inducing fibrosis [8, 40]. In addition, TNF- $\alpha$  contributes to the remodeling process through affecting variable mechanisms, such as angiotensin (Ang) II-mediated cardiac fibroblast responses, transforming growth factor beta (TGF- $\beta$ ), and cardiac fibroblast lysyl oxidase (LOX) expression, all of which induce myocardial fibrosis and dysfunction<sup>[63]</sup>. Remodeling is regarded initially, as a beneficial protective response but if left unopposed, it results in excessive collagen deposition and fibrosis. Moreover, sustained inflammation contributes to more damage to the myocardium<sup>[64]</sup>.

Histologically, evident collagen deposition was encountered in trichrome stained sections in group V (R) that proved statistically to be significantly increased as compared to all other groups. Such a result was supported ultra-structurally, where deposition of collagen fibrils was observed within the interstitium. Collagen deposition occurs as an integral part of the remodeling process of the myocardium.<sup>[64]</sup>

In addition, the role of metalloproteinases (MMPs), such as MMP-2 and MMP-9, in extracellular matrix (ECM) remodeling post MI, was investigated by previous research work. MMP-2 was proved to be implicated in degradation of type IV collagen found in the basement membrane and in denatured collagen, as well as other ECM proteins. Moreover, it aggravates the oxidative stress induced damage through derangement of mitochondrial respiration and membrane lipid peroxidation. MMP-9 is released from neutrophils and directly breaks down myocardium tissue or accentuates neutrophils infiltration, thus aggravating myocardium damage<sup>[40]</sup>. In this context, therapeutic intervention early post MI is mandatory.

The anti-inflammatory effect of BM-MSCs and EXO was evident histologically, where inflammatory cellular infiltration was limited in group IV (ST), whereas nearly not observed in group III (EXO). Biochemical results further confirmed such an effect, where tissue level of TNF- $\alpha$  was significantly decreased in both groups, with more decreased level demonstrated in group III (EXO). BM-MSCs mediate anti-inflammatory influence through local release of IL-1 receptor antagonist, thereby

suppressing TNF- $\alpha$  release by activated macrophages. Another effect is an immunomodulatory one via inhibition of T-cells proliferation and cytotoxicity or suppressing T-cell function by releasing TGF- $\beta$ <sup>[65]</sup>.

Moreover, previous research work has demonstrated that MSCs downregulate expression of inflammatory cytokines, such as IL 4 and proinflammatory cytokines such as IL 6, NF- $\kappa$ B, and MMP-3, meanwhile, increased expression of anti-inflammatory cytokine IL 10. The anti-inflammatory potential of EXO mimic their parent stem cell. In this context, it was demonstrated that administration of EXO ameliorated inflammation in experimentally induced acute spinal cord injury, where it was associated with increased expression of anti-inflammatory cytokine IL-10 and decreased in proinflammatory cytokines, such as TNF- $\alpha$  and IL-b. Consequently, modulating cardiac remodeling occurs with decreased fibrosis<sup>[66]</sup>. A significant anti-inflammatory role is related to IL-10, where it was demonstrated in literature that decreased IL-10 potentiates an exaggerated cardiac remodeling and fibrosis<sup>[67]</sup>. In this context, some exosomal mi-RNAs, such as, mi-RNA 18c and mi-RNA 466 I induce anti-inflammatory effect, by upregulating expression of IL-10<sup>[68,69]</sup>.

Additional therapeutic effect of BM-MSCs and EXO can be referred to their role in cardiac remodeling post MI. Such an effect of the transplanted stem cells is through secretion of regulatory ECM proteins, such as tissue inhibitor of MMP-1 that modulates activity of MMPs. Decreased formation of altered collagen I and III was also demonstrated. As such, BM-MSCs downregulates fibrosis<sup>[70]</sup>. Some other previous studies have demonstrated immunomodulatory role of mi-RNA 29 and mi-RNA 24 secreted either by the transplanted BM-MSCs or enclosed within the EXO, where mi-RNA 29 reduces fibrosis via downregulating collagen genes<sup>[71]</sup>. In such a context, the role of EXO in cardiac remodeling needs to be further elucidated. However, most previous studies outlined the role of different mi-RNAs, such as mi-RNA 22 that alleviates fibrosis with subsequent restoration of myocardial function<sup>[72]</sup>.

Angiogenesis is another therapeutic effect related to BM-MSCs and EXO, where impaired blood flow to the myocardium is one of the insults occurring in MI. BM-MSCs secrete different angiogenic mediators, such as vascular endothelial growth factor (VEGF), TGF- $\beta$  and basic fibroblast growth factor (bFGF)<sup>[73]</sup>.

Exosomes enhance such angiogenic effect upon systemic administration, where several mi-RNAs within the EXO possess angiogenic potential. Herein, mi-RNA 21 upregulates expression of VEGF, whereas mi-RNA 21-5p, additionally potentiates expression of TGF- $\beta$  signaling pathway. Moreover, TGF- $\beta$  and VEGF are among the EXO contents, that are considered to play a key role in angiogenesis<sup>[74]</sup>.

Level of TGF- $\beta$ 1 was assessed in the current work to evaluate its role in myocardial injury post ischemia and in

process of remodeling. Our assessment revealed interesting results, where significant increased level was documented in group II (ISO) in comparison to the control and all other groups, meanwhile both groups III (EXO) and IV (ST) revealed decreased levels of TGF- $\beta$ 1 as compared to groups II (ISO) and V (R). Here it should be clarified that the role of TGF- $\beta$ 1 in myocardial ischemia has been a debatable scientific issue. It is documented in literature that TGF- $\beta$  family is essential for normal development and functioning of cardiomyocytes<sup>[75]</sup>. Nevertheless, it was reported that ischemic cardiomyocytes and macrophages release TGF- $\beta$ 1, thereby increasing myocardium content of latent TGF- $\beta$ 1. However, the exact mechanism of its activation and initiation of signal transduction within cardiomyocytes has not been elucidated yet. Several hypothetical pathways have been suggested, involving interaction with proteases in matrix especially MMP, ROS generated during ischemia or extracellular matrix proteins<sup>[76,77]</sup>. However, its role in cardioprotection and remodeling is controversial. Some studies postulated that TGF- $\beta$ 1 might alleviate oxidative stress and downregulate release of inflammatory cytokines such as TNF- $\alpha$ <sup>[35]</sup>. Moreover, previous research work demonstrated that TGF- $\beta$ 1 might have a role in formation of myofibroblasts and expression of altered collagen within the matrix, thus contribute to myocardium fibrosis and remodeling<sup>[78]</sup>. Our results came in accordance with the aforementioned data, hereby explaining the robust increase in group II (ISO) and maintained elevated level in group V (R).

Our suggested interpretation for the decreased TGF- $\beta$ 1 levels in groups III (EXO) and IV (ST) is based on the therapeutic effects mediated by exosomes and stem cells, which restore the endogenous antioxidant balance and ameliorate the inflammatory response, thus maintaining TGF- $\beta$ 1 in its latent form. However, exosomes and stem cells still represent a potential source for TGF- $\beta$ 1.<sup>[78]</sup>

## CONCLUSION

The current study emphasized that exosomes possess a distinguished therapeutic potential as compared to BM-MSCs on isoproterenol induced ventricular myocardium changes in adult rats, where they successfully restored structural integrity of the myocardium. Thus, MSCs derived exosomes are regarded as a promising therapeutic strategy in myocardial infarction. However, more research work is recommended to investigate the maintained therapeutic potential over time in correlation to structural integrity and functional efficiency.

## ETHICAL STATEMENT

The animal studies were performed after receiving approval of the institutional review board of ethics, Faculty of Medicine, Alexandria University.

## ACKNOWLEDGEMENTS

The authors appreciate the supportive role of the Faculty of Medicine, Alexandria University.

## CONFLICT OF INTERESTS

There are no conflicts of interest.

## REFERENCES

1. Nowbar AN, Gitto M, Howard JP, Francis DP and Al-Lamee R: Mortality From Ischemic Heart Disease. *Circ Cardiovasc Qual Outcomes* (2019) 12(6):e005375.
2. D'Oria R, Schipani R, Leonardini A, Natalicchio A, Perrini S, Cignarelli A, Laviola L and Giorgino F: The Role of Oxidative Stress in Cardiac Disease: From Physiological Response to Injury Factor. *Oxid Med Cell Longev* (2020) 2020:5732956.
3. Kain V, Prabhu SD and Halade GV: Inflammation revisited: inflammation versus resolution of inflammation following myocardial infarction. *Basic Res Cardiol* (2014) 109(6):444.
4. Sandoval Y and Jaffe AS: Type 2 Myocardial Infarction: JACC Review Topic of the Week. *J Am Coll Cardiol* (2019) 73(14):1846-1860.
5. DeFilippis AP, Chapman AR, Mills NL, de Lemos JA, Arbab-Zadeh A, Newby LK and Morrow DA: Assessment and Treatment of Patients With Type 2 Myocardial Infarction and Acute Nonischemic Myocardial Injury. *Circulation* (2019) 140(20):1661-1678.
6. Forte E, Panahi M, Baxan N, *et al*: Type 2 MI induced by a single high dose of isoproterenol in C57BL/6J mice triggers a persistent adaptive immune response against the heart. *J Cell Mol Med* (2021) 25(1):229-243.
7. Procaccini DE, Sawyer JE and Watt KM: Pharmacology of Cardiovascular drugs. In: Ungerleider RM, Meliones JN, McMillan KN, Cooper DS and Jacobs JP (eds). *Critical Heart Disease in Infants and Children*. 3rd ed. Elsevier. Philadelphia. (2019) p.p: 192-212.
8. Sahu BD, Kuncha M, Rachamalla SS and Sistla R: *Lagerstroemia speciosa* L. attenuates apoptosis in isoproterenol-induced cardiotoxic mice by inhibiting oxidative stress: possible role of Nrf2/HO-1. *Cardiovasc Toxicol* (2015) 15(1):10-22.
9. Caccioppo A, Franchin L, Grosso A, Angelini F, D'Ascenzo F and Brizzi MF: Ischemia Reperfusion Injury: Mechanisms of Damage/Protection and Novel Strategies for Cardiac Recovery/Regeneration. *Int J Mol Sci* (2019) 20(20):5024.
10. Tompkins BA, Balkan W, Winkler J, Gyöngyösi M, Goliash G, Fernández-Avilés F and Hare JM: Preclinical Studies of Stem Cell Therapy for Heart Disease. *Circ Res* (2018) 122(7):1006-1020.
11. Afzal MR, Samanta A, Shah ZI, Jeevanantham V, Abdel-Latif A, Zuba-Surma EK and Dawn B: Adult Bone Marrow Cell Therapy for Ischemic Heart Disease: Evidence and Insights From Randomized Controlled Trials. *Circ Res* (2015) 117(6):558-575.

12. Sahoo S, Adamiak M, Mathiyalagan P, Kenneweg F, Kafert-Kasting S and Thum T: Therapeutic and Diagnostic Translation of Extracellular Vesicles in Cardiovascular Diseases: Roadmap to the Clinic. *Circulation* (2021) 143(14):1426-1449.
13. Cai M, Shen R, Song L, *et al*: Bone Marrow Mesenchymal Stem Cells (BM-MSCs) Improve Heart Function in Swine Myocardial Infarction Model through Paracrine Effects. *Sci Rep* (2016) 6:28250.
14. Zhang CS, Shao K, Liu CW, Li CJ and Yu BT: Hypoxic preconditioning BMSCs-exosomes inhibit cardiomyocyte apoptosis after acute myocardial infarction by upregulating microRNA-24. *Eur Rev Med Pharmacol Sci* (2019) 23(15):6691-6699.
15. Chen GH, Xu J and Yang YJ: Exosomes: promising sacks for treating ischemic heart disease? *Am J Physiol Heart Circ Physiol* (2017) 313(3):H508-h523.
16. Tan SJO, Floriano JF, Nicastro L, Emanuelli C and Catapano F: Novel Applications of Mesenchymal Stem Cell-derived Exosomes for Myocardial Infarction Therapeutics. *Biomolecules* (2020) 10(5): 707-737.
17. Li W, Zeng J, Zhu G, Dong Y, Xie D and Lai R: In *Vitro* Cultivation Technology of Rat Bone Marrow Mesenchymal Stem Cells. *Journal of Biomaterials and Tissue Engineering* (2019) 9:62-68.
18. Ghaneialvar H, Soltani L, Rahmani HR, Lotfi AS and Soleimani M: Characterization and Classification of Mesenchymal Stem Cells in Several Species Using Surface Markers for Cell Therapy Purposes. *Indian J Clin Biochem* (2018) 33(1):46-52.
19. Penfornis P and Pochampally R: Colony forming unit assays. In: Penfornis P and Pochampally R (eds). *Mesenchymal stem cells*. Springer. Berlin. (2016) p.p: 159-169.
20. Xu J, Xiong Y-Y, Li Q, *et al*: Optimization of Timing and Times for Administration of Atorvastatin-Pretreated Mesenchymal Stem Cells in a Preclinical Model of Acute Myocardial Infarction. *Stem cells translational medicine* (2019) 8(10):1068-1083.
21. Greening DW, Xu R, Ji H, Tauro BJ and Simpson RJ: A protocol for exosome isolation and characterization: evaluation of ultracentrifugation, density-gradient separation, and immunoaffinity capture methods. *Methods Mol Biol* (2015) 1295:179-209.
22. Walker JM: The Bicinchoninic Acid (BCA) Assay for Protein Quantitation. In: (eds) WJM (ed). *The Protein Protocols Handbook: Springer Protocols Handbooks*. Humana Press. London. (1996) p.p: 11-15.
23. Smith ZJ, Lee C, Rojalin T, *et al*: Single exosome study reveals subpopulations distributed among cell lines with variability related to membrane content. *J Extracell Vesicles* (2015) 4:28533.
24. Xu R, Greening DW, Zhu HJ, Takahashi N and Simpson RJ: Extracellular vesicle isolation and characterization: toward clinical application. *J Clin Invest* (2016) 126(4):1152-1162.
25. Mohammadi MR, Riazifar M, Pone EJ, Yeri A, Van Keuren-Jensen K, Lässer C, Lotvall J and Zhao W: Isolation and characterization of microvesicles from mesenchymal stem cells. *Methods* (2020) 177:50-57.
26. Li H, Song F, Duan LR, *et al*: Paeonol and danshensu combination attenuates apoptosis in myocardial infarcted rats by inhibiting oxidative stress: Roles of Nrf2/HO-1 and PI3K/Akt pathway. *Sci Rep* (2016) 6:23693.
27. Xiao M, Zeng W, Wang J, *et al*: Exosomes Protect Against Acute Myocardial Infarction in Rats by Regulating the Renin-Angiotensin System. *Stem Cells Dev* (2021) 30(12):622-631.
28. Li N, Yang Y-J, Qian H-Y, *et al*: Intravenous administration of atorvastatin-pretreated mesenchymal stem cells improves cardiac performance after acute myocardial infarction: role of CXCR4. *American journal of translational research* (2015) 7(6):1058-1070.
29. Struck MB, Andrutis KA, Ramirez HE and Battles AH: Effect of a short-term fast on ketamine-xylazine anesthesia in rats. *J Am Assoc Lab Anim Sci* (2011) 50(3):344-348.
30. White HD: Pathobiology of troponin elevations: do elevations occur with myocardial ischemia as well as necrosis? *J Am Coll Cardiol* (2011) 57(24):2406-2408.
31. Wu Y-W, Ho SK, Tseng W-K, *et al*: Potential impacts of high-sensitivity creatine kinase-MB on long-term clinical outcomes in patients with stable coronary heart disease. *Scientific reports* (2020) 10(1):5638-5638.
32. Tsikas, D. Assessment of lipid peroxidation by measuring malondialdehyde (MDA) and relatives in biological samples: Analytical and biological challenges. *Anal Biochem.* (2017) 524:13-30.
33. Kinnunen S, Hyypää S, Lehmuskero A, Oksala N, Mäenpää P, Hänninen O and Atalay M: Oxygen radical absorbance capacity (ORAC) and exercise-induced oxidative stress in trotters. *Eur J Appl Physiol* (2005) 95(5-6):550-556.
34. Kishore R, Tkebuchava T, Sasi SP, *et al*: Tumor necrosis factor- $\alpha$  signaling via TNFR1/p55 is deleterious whereas TNFR2/p75 signaling is protective in adult infarct myocardium. *Adv Exp Med Biol* (2011) 691:433-448.
35. Hanna A and Frangogiannis NG: The Role of the TGF- $\beta$  Superfamily in Myocardial Infarction. *Front Cardiovasc Med* (2019) 6:140-155.

36. Bancroft J and Layton C: The hematoxylin and eosin, connective and mesenchymal tissues with their stains. In: Suvarna S, Layton C and Bancroft J (eds). Bancroft's Theory and Practice of Histological Techniques. 7th ed. Churchill Livingstone. Philadelphia. (2013) p.p: 173-212.
37. Graham R, Gray T, Bancroft J and Stevens A: Electron microscopy 2: practical procedures. In: Bancroft JD and Stevens A (eds). Theory and Practice of Histological Techniques 4th. Churchill-Livingstone. New York. (1996) p.p: 101-123.
38. Kobayashi T, Masumoto J, Tada T, Nomiyama T, Hongo K and Nakayama J: Prognostic significance of the immunohistochemical staining of cleaved caspase-3, an activated form of caspase-3, in gliomas. Clin Cancer Res (2007) 13(13):3868-3874.
39. Kotz S, Balakrishnan N, Read C and Vidakovic B: Encyclopedia of statistical sciences. 2nd ed., Wiley-Interscience. Hoboken, N.J. (2006) p.p 8371-8377.
40. Boarescu P-M, Chirilă I, Bulboacă AE, Bocșan IC, Pop RM, Gheban D and Bolboacă SD: Effects of curcumin nanoparticles in isoproterenol-induced myocardial infarction. Oxidative medicine and cellular longevity (2019) 2019:7847142.
41. Starnberg K, Fridén V, Muslimovic A, *et al*: A Possible Mechanism behind Faster Clearance and Higher Peak Concentrations of Cardiac Troponin I Compared with Troponin T in Acute Myocardial Infarction. Clin Chem (2020) 66(2):333-341.
42. Sivasangari S, Asaikumar L and Vennila L: Arbutin prevents alterations in mitochondrial and lysosomal enzymes in isoproterenol-induced myocardial infarction: An *in vivo* study. Human & Experimental Toxicology (2021) 40(1):100-112.
43. Chen H, Xu Y, Wang J, Zhao W and Ruan H: Baicalin ameliorates isoproterenol-induced acute myocardial infarction through iNOS, inflammation and oxidative stress in rat. Int J Clin Exp Pathol (2015) 8(9):10139-10147.
44. Jain PG, Mahajan UB, Shinde SD and Surana SJ: Cardioprotective role of FA against isoproterenol induced cardiac toxicity. Mol Biol Rep (2018) 45(5):1357-1365.
45. Asaikumar L, Vennila L, Akila P, Sivasangari S, Kanimozhi K, Premalatha V and Sindhu G: Expression of Concern: Preventive effect of nerolidol on isoproterenol induced myocardial damage in Wistar rats: Evidences from biochemical and histopathological studies. Drug Development Research (2019) 80(6):814-823.
46. Maleki Dizaji N, Garjani A, Mousavi S, Mohammadi M and Vaez H: Time-dependent influence of infliximab on hemodynamic responses and cardiac injuries of isoproterenol-induced myocardial infarction in rats. Eur J Pharmacol (2021) 903:174122.
47. Saranya S, Baskaran R, Poornima P and Vijaya Padma V: Berbamine ameliorates isoproterenol-induced myocardial infarction by inhibiting mitochondrial dysfunction and apoptosis in rats. Journal of Cellular Biochemistry (2019) 120(3):3101-3113.
48. Meeran MFN, Laham F, Al-Tae H, Azimullah S and Ojha S: Protective effects of  $\alpha$ -bisabolol on altered hemodynamics, lipid peroxidation, and nonenzymatic antioxidants in isoproterenol-induced myocardial infarction: *In vivo* and *in vitro* evidences. Journal of Biochemical and Molecular Toxicology (2018) 32(10):e22200.
49. Hassan MQ, Akhtar MS, Akhtar M, Ali J, Haque SE and Najmi AK: Edaravone protects rats against oxidative stress and apoptosis in experimentally induced myocardial infarction: Biochemical and ultrastructural evidence. Redox Rep (2015) 20(6):275-281.
50. Gardiner C, Di Vizio D, Sahoo S, Théry C, Witwer KW, Wauben M and Hill AF: Techniques used for the isolation and characterization of extracellular vesicles: results of a worldwide survey. J Extracell Vesicles (2016) 5:32945.
51. Jeppesen DK, Hvam ML, Primdahl-Bengtson B, Boysen AT, Whitehead B, Dyrskjøt L, Orntoft TF, Howard KA and Ostfeldt MS: Comparative analysis of discrete exosome fractions obtained by differential centrifugation. J Extracell Vesicles (2014) 3:25011.
52. Chen Q, Liu Y, Ding X, Li Q, Qiu F, Wang M, Shen Z, Zheng H and Fu G: Bone marrow mesenchymal stem cell-secreted exosomes carrying microRNA-125b protect against myocardial ischemia reperfusion injury via targeting SIRT7. Molecular and cellular biochemistry (2020) 465(1-2):103-114.
53. Hodgkinson CP, Bareja A, Gomez JA and Dzau VJ: Emerging Concepts in Paracrine Mechanisms in Regenerative Cardiovascular Medicine and Biology. Circ Res (2016) 118(1):95-107.
54. Gneccchi M, Danieli P, Malpasso G and Ciuffreda MC: Paracrine Mechanisms of Mesenchymal Stem Cells in Tissue Repair. Methods Mol Biol (2016) 1416:123-146.
55. Reis M, Ogonek J, Qesari M, *et al*: Recent Developments in Cellular Immunotherapy for HSCT-Associated Complications. Front Immunol (2016) 7:500.
56. Cheng Y, Wang X, Yang J, *et al*: A translational study of urine miRNAs in acute myocardial infarction. J Mol Cell Cardiol (2012) 53(5):668-676.
57. Gneccchi M, He H, Noiseux N, *et al*: Evidence supporting paracrine hypothesis for Akt-modified mesenchymal stem cell-mediated cardiac protection and functional improvement. Faseb j (2006) 20(6):661-669.

58. Wang X, Pan J, Liu D, Zhang M, Li X, Tian J, Liu M, Jin T and An F: Nicorandil alleviates apoptosis in diabetic cardiomyopathy through PI3K/Akt pathway. *Journal of cellular and molecular medicine* (2019) 23(8):5349-5359.
59. Chen C-H, Hsu S-Y, Chiu C-C and Leu S: MicroRNA-21 Mediates the Protective Effect of Cardiomyocyte-Derived Conditioned Medium on Ameliorating Myocardial Infarction in Rats. *Cells* (2019) 8(8):935.
60. Arslan F, Lai RC, Smeets MB, *et al*: Mesenchymal stem cell-derived exosomes increase ATP levels, decrease oxidative stress and activate PI3K/Akt pathway to enhance myocardial viability and prevent adverse remodeling after myocardial ischemia/reperfusion injury. *Stem Cell Res* (2013) 10(3):301-312.
61. Yu X, Deng L, Wang D, *et al*: Mechanism of TNF- $\alpha$  autocrine effects in hypoxic cardiomyocytes: initiated by hypoxia inducible factor 1 $\alpha$ , presented by exosomes. *J Mol Cell Cardiol* (2012) 53(6):848-857.
62. Meeran MFN, Azimullah S, Adeghate E and Ojha S: Nootkatone attenuates myocardial oxidative damage, inflammation, and apoptosis in isoproterenol-induced myocardial infarction in rats. *Phytomedicine* (2021) 84:153405.
63. Van Linthout S and Tschöpe C: Inflammation - Cause or Consequence of Heart Failure or Both? *Curr Heart Fail Rep* (2017) 14(4):251-265.
64. Cochain C, Auvynet C, Poupel L, *et al*: The chemokine decoy receptor D6 prevents excessive inflammation and adverse ventricular remodeling after myocardial infarction. *Arterioscler Thromb Vasc Biol* (2012) 32(9):2206-2213.
65. Shafei AE, Ali MA, Ghanem HG, Shehata AI, Abdelgawad AA, Handal HR, Talaat KA, Ashaal AE and El-Shal AS: Mesenchymal stem cell therapy: A promising cell-based therapy for treatment of myocardial infarction. *J Gene Med* (2017) 19(12).
66. Huang JH, Yin XM, Xu Y, Xu CC, Lin X, Ye FB, Cao Y and Lin FY: Systemic Administration of Exosomes Released from Mesenchymal Stromal Cells Attenuates Apoptosis, Inflammation, and Promotes Angiogenesis after Spinal Cord Injury in Rats. *J Neurotrauma* (2017) 34(24):3388-3396.
67. Verma SK, Krishnamurthy P, Barefield D, *et al*: Interleukin-10 treatment attenuates pressure overload-induced hypertrophic remodeling and improves heart function via signal transducers and activators of transcription 3-dependent inhibition of nuclear factor- $\kappa$ B. *Circulation* (2012) 126(4):418-429.
68. Li X, Liu L, Yang J, Yu Y, Chai J, Wang L, Ma L and Yin H: Exosome Derived From Human Umbilical Cord Mesenchymal Stem Cell Mediates MiR-181c Attenuating Burn-induced Excessive Inflammation. *EBioMedicine* (2016) 8:72-82.
69. Ma F, Liu X, Li D, Wang P, Li N, Lu L and Cao X: MicroRNA-466l upregulates IL-10 expression in TLR-triggered macrophages by antagonizing RNA-binding protein tristetraprolin-mediated IL-10 mRNA degradation. *J Immunol* (2010) 184(11):6053-6059.
70. Gubert F, da Silva JS, Vasques JF, de Jesus Gonçalves RG, Martins RS, de Sá MPL, Mendez-Otero R and Zapata-Sudo G: Mesenchymal Stem Cells Therapies on Fibrotic Heart Diseases. *International journal of molecular sciences* (2021) 22(14):7447.
71. Wang B, Komers R, Carew R, *et al*: Suppression of microRNA-29 expression by TGF- $\beta$ 1 promotes collagen expression and renal fibrosis. *J Am Soc Nephrol* (2012) 23(2):252-265.
72. Feng Y, Huang W, Wani M, Yu X and Ashraf M: Ischemic preconditioning potentiates the protective effect of stem cells through secretion of exosomes by targeting Mecp2 via miR-22. *PLoS One* (2014) 9(2):e88685.
73. Anderson JD, Johansson HJ, Graham CS, *et al*: Comprehensive Proteomic Analysis of Mesenchymal Stem Cell Exosomes Reveals Modulation of Angiogenesis via Nuclear Factor-KappaB Signaling. *Stem Cells* (2016) 34(3):601-613.
74. Collino F, Pomatto M, Bruno S, Lindoso RS, Tapparo M, Sicheng W, Quesenberry P and Camussi G: Exosome and Microvesicle-Enriched Fractions Isolated from Mesenchymal Stem Cells by Gradient Separation Showed Different Molecular Signatures and Functions on Renal Tubular Epithelial Cells. *Stem Cell Rev Rep* (2017) 13(2):226-243.
75. Umbarkar P, Singh AP, Gupte M, *et al*: Cardiomyocyte SMAD4-Dependent TGF- $\beta$  Signaling is Essential to Maintain Adult Heart Homeostasis. *JACC Basic Transl Sci* (2019) 4(1):41-53.
76. Spinale FG: Myocardial matrix remodeling and the matrix metalloproteinases: influence on cardiac form and function. *Physiol Rev* (2007) 87(4):1285-1342.
77. Liu CL, Guo J, Zhang X, Sukhova GK, Libby P and Shi GP: Cysteine protease cathepsins in cardiovascular disease: from basic research to clinical trials. *Nat Rev Cardiol* (2018) 15(6):351-370.
78. Shinde AV and Frangogiannis NG: Mechanisms of Fibroblast Activation in the Remodeling Myocardium. *Curr Pathobiol Rep* (2017) 5(2):145-152.

## الملخص العربي

## التأثير العلاجي للخلايا الجذعية الوسيطة المشتقة من نخاع العظم في مقابل حويصلاتها على تغيرات عضلة بطين القلب المحدثه بالأيزوبروتيرينول في الجرذان البالغة: دراسة نسيجية ونسجية كيميائية مناعية وكيميائية حيوية

أماني عبد المنعم سليمان ورحاب أحمد عبد المنعم

قسم الهستولوجيا وبيولوجيا الخلية، كلية الطب، جامعة الإسكندرية

**المقدمة:** يمثل احتشاء عضلة القلب حالة تهدد الحياة. تتضمن اسبابها توليد الأوكسجين التفاعلي و نقص الاوكسوجين. ان التدخل العلاجي الفوري للخلايا الجذعية الوسيطة المشتقة من نخاع العظم او الحويصلات المستخرجة منها قد سبق دراستها نظرا لآثارها العلاجية المحتملة لتجنب تليف القلب وإعادة هيكلته.

**الهدف:** البحث في الإمكانية العلاجية للخلايا الجذعية الوسيطة المشتقة من نخاع العظم في مقابل الحويصلات المستخرجة منها للتأثير على تغيرات عضلة القلب المحدثه بالأيزوبروتيرينول (أيزو) في نموذجاً للجرذان.

**طرق البحث:** تم تقسيم ٣٢ جرذاً من ذكور الجرذان البيضاء البالغة إلى خمسة مجموعات: المجموعة الضابطة، مجموعة (أيزو) والتي تم حقنها ب أيزو بجرعة ٨٥ مجم / كجم من وزن الجسم تحت الجلد مرتين بفاصل ٢٤ ساعة، وتم ذبحها بعد ٢٤ ساعة من آخر جرعة.

مجموعة الحويصلات و مجموعة الخلايا الجذعية المشتقة، تم حقنها عبر الوريد في الذيل ب ١٠٠ ميكروغرام من الحويصلات و \*١٠٦١,٢ من الخلايا الجذعية المشتقة، بعد ٢٤ ساعة من آخر جرعة من أيزو وتم الذبح بعد أربعة أسابيع. تم حقن مجموعة الاسترداد بأيزو تركها لمدة ٤ أسابيع بعد آخر جرعة من ال أيزو ثم ذبحها. تمت تجهيز و فحص عينات من البطين الأيسر للتقييم النسيجي باستخدام المجهر الضوئي والإلكتروني. كما تضمنت الدراسة التقييم النسيجي الكيميائي المناعي لمضاد caspase-٣. تم تقييم مالونديالديهيد، السعة الكلية لمضادات الأوكسدة، عامل نخر الورم- ألفا وتحويل عامل النمو بيتا ١ في متجانسات أنسجة البطين الأيمن. تم أيضاً تقييم تروبونين ١ وكرياتين كيناز في المصل.

**النتائج:** من الناحية النسيجية، كشفت مجموعة ال أيزو عن تغيرات تنكسية متغيرة في شكل انحلال الخلايا العضلية والتسلل الخلوي وتغيرات بالنوي. وقد زاد مستوي كل من التروبونين ١ والكرياتين كيناز في السيروم بشكل ملحوظ. وقد وجد زيادة كبيرة في التفاعل النسيجي الكيميائي المناعي لمضاد caspase-٣. كشفت كل من مجموعات الحويصلات والخلايا الجذعية عن تحسن في معايير التقييم المختلفة والتي كانت أكثر وضوحاً في المجموعة المعالجة بالحويصلات. **استنتاج:** أثبتت هذه الدراسة أن للحويصلات تأثيراً علاجياً أكثر فاعلية من الخلايا الجذعية الوسيطة المشتقة من نخاع العظم على التغيرات المحدثه بال أيزو في عضلة البطين ، وبالتالي تعتبر الحويصلات المستخرجة من الخلايا الجذعية الوسيطة استراتيجية واعدة في علاج احتشاء عضلة القلب.